



**Gesellschaft für Anlagen-  
und Reaktorsicherheit  
(GRS) mbH**

**Geoelectric  
Investigation of  
Bentonite Barrier  
Saturation**



**Gesellschaft für Anlagen-  
und Reaktorsicherheit  
(GRS) mbH**

## **Geoelectric Investigation of Bentonite Barrier Saturation**

Conducted in the  
Prototype Repository at  
the Äspö Hard Rock  
Laboratory

Tilmann Rothfuchs  
Rüdiger Miehe  
Helge Moog  
Klaus Wiczorek

November 2004

### **Remark:**

This report was prepared under contract No. 02 E 9279 with the Bundesministerium für Wirtschaft und Arbeit (BMWA) and under contract No. FIKW-CT-2000-00055 with the European Commission.

The work was conducted by the Gesellschaft für Anlagen- und Reaktorsicherheit (GRS) mbH.

The authors are responsible for the content of this report.

**GRS - 208  
ISBN 3-931995-75-5**

**Deskriptoren:**

Deutschland, Endlager, Elektrochemie, Felsformation, Geoelektrik, Langzeitsicherheit, Meßwert, Schweden, Wärme, Wiederauffüllung

## Foreword

Within the framework of the Swedish nuclear programme, SKB has constructed a full-scale replica of the deep repository planned for the disposal of spent nuclear fuel. This Prototype Repository has been constructed at the Äspö Hard Rock Laboratory at a depth of 450 m below ground. The Prototype includes six deposition holes in which full-size canisters with electrical heaters have been placed and surrounded by a bentonite buffer. The deposition tunnel has been backfilled with a mixture of bentonite and crushed granitic rock.

Water uptake of the bentonite buffer in the deposition holes and of the bentonite/crushed rock backfill in the disposal gallery is one of the central issues to be investigated in the frame of the Prototype Repository Project performed at the Äspö URL. GRS uses the geoelectric method to monitor changes in water content, as the electric resistivity of the materials is determined by the solution content. Several electrode arrays in the buffer, the backfill, and the rock serve for determining the resistivity distributions in cross sections of the different materials. From the resistivity the solution content can be derived using the results of calibration measurements on samples at defined conditions.

This document representing an interim report on the measurements performed by GRS between October 2001 and February 2004 comprises a brief description of the theoretical principles of DC-geoelectrics and the applied field measurements techniques, of the arrangement of the measuring arrays in the Prototype Repository, of the laboratory calibrations performed at GRS' geotechnical laboratory in Braunschweig, and the actual measuring results obtained until the end of February 2004.

The work was performed under contract No. 02 E 9279 with the Projektträger Wasser-technologie und Entsorgung (PtWT+E) of the German Ministry for Economics and Labour (BMWA) in the time period from 1 January 2000 until 29 February 2004.

The project was co-funded under contract No. FIKW-CT-2000-00055 by the European Commission (EC) in the time period from 1 September 2000 until 29 February 2004.

## Table of Contents

	<b>Foreword</b> .....	<b>I</b>
	<b>Table of Contents</b> .....	<b>III</b>
<b>1</b>	<b>Introduction</b> .....	<b>1</b>
<b>2</b>	<b>Theoretical Principles</b> .....	<b>3</b>
<b>3</b>	<b>Monitoring System</b> .....	<b>7</b>
3.1	Measuring Techniques.....	7
3.2	Measurement Evaluation .....	8
3.3	Measurement System .....	9
3.3.1	Hardware Components .....	10
3.3.2	Resistivity Meter and Embedded PC .....	10
3.3.3	Injection Voltage Supply.....	13
3.3.4	Electrode Decoder Array .....	14
3.3.5	Uninterruptable Power Supply .....	15
3.3.6	Measuring Procedure.....	15
<b>4</b>	<b>Measuring Arrays in the Prototype Repository</b> .....	<b>17</b>
4.1	Backfill.....	17
4.2	Buffer.....	17
4.3	Rock .....	18
4.4	Electrodes and Electrode Chains.....	18
<b>5</b>	<b>Laboratory Calibration</b> .....	<b>27</b>
5.1	Resistivity of MX-80-Bentonite .....	27
5.1.1	Samples .....	27
5.1.2	Measurement and Evaluation .....	29
5.1.3	Results .....	30
5.2	Drift Backfill .....	33
5.2.1	Samples .....	33

5.2.2	Results .....	34
5.3	Rock .....	36
5.4	Cementation Material .....	40
5.4.1	Samples .....	41
5.4.2	Measurement and Evaluation .....	41
5.4.3	Results .....	42
5.5	Change of Composition of Äspö-Solution by Interaction with Compacted MX-80 .....	44
5.5.1	Materials and Methods .....	45
5.5.2	Results .....	47
<b>6</b>	<b>Assessment of Measurement Resolution .....</b>	<b>57</b>
6.1	Backfill .....	57
6.2	Buffer .....	60
<b>7</b>	<b>Field Measurements .....</b>	<b>63</b>
7.1	Backfill Section I .....	63
7.2	Backfill Section II .....	65
7.3	Buffer .....	66
7.4	Rock .....	67
<b>8</b>	<b>Summary and Conclusions .....</b>	<b>71</b>
<b>9</b>	<b>Acknowledgements .....</b>	<b>75</b>
<b>10</b>	<b>References .....</b>	<b>77</b>
	<b>List of Figures .....</b>	<b>81</b>
	<b>List of Tables .....</b>	<b>85</b>

# 1 Introduction

Within the framework of the Prototype Repository Project performed by the Svensk Kärnbränslehantering AB (SKB) at the Aespoe Hard Rock Laboratory (HRL) in Sweden six copper casks containing electrical heaters have been emplaced in deposition boreholes drilled into the floor of a drift at 450 m depth below ground. The gap between the casks and the crystalline rock has been filled with Na-bentonite buffer. The drift above the deposition boreholes has been backfilled, too, with a mixture consisting of 30 % bentonite and 70 % crushed rock.

The rock, the buffer, and the backfill have been instrumented by SKB for recording temperatures, swelling and water pressures. In addition to that, multi-electrode arrays have been installed by the Gesellschaft für Anlagen- und Reaktorsicherheit (GRS) at the top of one deposition borehole, in the drift above the deposition boreholes, and in the rock between two of the deposition boreholes in order to determine water uptake in the buffer and the backfill and possible desaturation of the rock by geoelectric measurements.

In the geoelectric measurements advantage is taken of the dependence of the electrical resistivity of rocks on the water (solution) content. In order to interpret measured resistivity in terms of water content, the field measurements have been accompanied by laboratory calibration measurements.

Besides its dependence on the water content, the electrical resistivity is also a function of salinity and composition of the pore solution. Since both may change as the solution penetrates the buffer and the backfill, respective laboratory investigations were performed in order to quantify this effect.

On basis of the results of the laboratory investigations model calculations have been performed to determine the achievable measuring resolution and to determine optimized electrode configurations in the areas to be surveyed.

The laboratory calibrations were performed in the time period from January 2000 until February 2003. The electrode arrays were installed according to the progress of test equipment installation in the deposition boreholes and the test drift in the time period from October 2001 until June 2003. First measurements were started in the backfill in section I in October 2001. The last array in the backfill in section II was taken into

operation in June 2003. It is envisaged to continue the measurements for a further time period lasting from August 2004 until July 2007.

## 2 Theoretical Principles

In direct current geoelectrics, a stationary electric field is generated in a dielectric by means of two current electrodes and is measured with two further potential electrodes.

In an isotropic medium, the current density  $J$  generated by an electric field  $E$  is described by the constitutive equation (Ohm's law),

$$J = \sigma E \quad (1)$$

With the exception of laboratory measurements on test samples of known geometry, the electrical conductivity  $\sigma$  is not directly measurable. The value determined by field measurements depends on the geometry of the measuring arrangement and is affected by the inhomogeneity of the structure; it is therefore designated as the apparent electrical conductivity. In practice, the electrical resistivity, that is, the reciprocal of the conductivity, is more frequently employed and is denoted by  $\rho = 1/\sigma$ .

In the case of a uniform electric current,  $\text{rot } E$  vanishes:

$$\text{rot } E = 0 \quad (2)$$

From Maxwell's equations, it thus follows that the magnetic field is constant:

$$\partial B / \partial t = 0 \quad (3)$$

Equation (13) indicates that  $E$  can be expressed as the gradient of a scalar potential  $\psi$ :

$$E = -\text{grad } \psi \quad (4)$$

This potential is sufficient because  $\text{div } J = \text{div } (\sigma E)$  in the differential equation:

$$\sigma \text{ div grad } \psi = -\text{div } J \quad (5)$$

In accordance with Gauss' theorem of vector analysis, the volume integral of the divergence of the current density  $J$  over the volume  $V$  is equal to the sum of the current sources within the volume  $V$ :

$$\int_V \text{div } J \, dV = I \delta \quad (6)$$

$\delta$  is the Dirac delta function, which assumes the value 1 where sources are present and is otherwise equal to zero. For an infinitesimally small volume  $dV$ , the following applies:

$$\text{div } J = I \delta \quad (7)$$

In accordance with (5),

$$\text{div } J = -\sigma \text{ div grad } \psi \quad (8)$$

applies; hence, Poisson's differential equation is finally obtained for the potential field due to arbitrary current sources:

$$\text{div grad } \psi = -\rho I \delta \quad (9)$$

with  $\rho = 1/\sigma$ .

If it is assumed that the electric field is stationary,  $E$  can be derived as an irrotational vector from a potential  $\psi$ . If the divergence is determined from (4), the following inhomogeneous potential equation is obtained for  $\psi$ :

$$\text{div grad } \psi = -\text{div } E \quad (10)$$

The right-hand side of this equation is known. With the application of Green's theorem from vector analysis,  $\psi$  can be calculated in the following form:

$$4 \pi \psi = \int_V \frac{\text{div } E}{r} \, dV \quad (11)$$

With the use of equations 11, 10, and 9, the potential field  $\psi$  is thus obtained for a point source:

$$\psi = \frac{1}{4\pi} I \rho \frac{1}{r} \quad (12)$$

$I$  is the current which flows through the source, and  $r$  is the distance of the point under consideration from the source point for which  $\psi$  is being calculated and over whose coordinates the integration is being performed. The source point is also the location of the volume element  $dV$ . The potential field of a dipole source results from the superposition of the potential fields for two point sources with positive and negative current:

$$\psi = \psi_1 + \psi_2 = \frac{1}{4\pi} I \rho \left( \frac{1}{r_1} - \frac{1}{r_2} \right) \quad (13)$$

$r_1$  and  $r_2$  denote the distances of the points under consideration from source points 1 and 2, respectively, with the potential fields  $\psi_1$  and  $\psi_2$ . The potential field generated by the dipole source is measured as a potential difference at two potential electrodes. If equation (13) is applied at each potential probing point, and if the difference is calculated, the following is obtained:

$$\Delta\psi = \frac{1}{4\pi} I \rho \left( \frac{1}{r_{11}} - \frac{1}{r_{12}} - \frac{1}{r_{21}} + \frac{1}{r_{22}} \right) \quad (14)$$

$r_{ij}$  is the distance of the  $i_{th}$  potential electrode from the  $j_{th}$  current electrode. The expression between brackets is denoted by  $1/K$  for brevity.  $K$  is designated as a geometric factor.

During a measurement, the potential difference as well as the current supplied are measured, and the resistance is determined. This value is the sum of the resistances between the current electrodes and the contact resistances at the electrodes; it is an apparent resistance. The true resistivity is equal to the apparent resistivity only in a homogeneous medium. The apparent resistivity is given by:

$$\rho = 4\pi \frac{\Delta\psi}{I} K \quad (15)$$

In geoelectrics, a wide variety of electrode arrangements are employed. The Wenner arrangement is worthy of special mention; in this four-point arrangement with equal electrode spacing  $a$ , the electrodes lie in a straight line. The outer electrodes are the current electrodes, and the inner electrodes are the potential electrodes. Since  $r_{11} = r_{22} = a$  and  $r_{12} = r_{21} = 2a$  apply, equation (14) yields the geometric factor as follows:

$$K = \frac{1}{\frac{1}{r_{11}} - \frac{1}{r_{12}} - \frac{1}{r_{21}} + \frac{1}{r_{22}}} = a \quad (16)$$

In this expression,  $a$  is the electrode spacing in a Wenner arrangement.

As a rule, geoelectrics is applied on profiles at the earth's surface, where the factor  $4\pi$  (three-dimensional space) in (15) is replaced by the factor  $2\pi$  (half-space); that is, the problem under investigation is two-dimensional. In three-dimensional space, the electrodes are spatially distributed, either in an array on the surface or in boreholes. Special care is necessary for the calculation of the geometric factor, since it may possess poles, which must be taken into account during the measurements.

### 3 Monitoring System

#### 3.1 Measuring Techniques

The technique most frequently applied for geoelectric measurements in the field is the four-point method (Figure 3-1). An electric current is supplied to the formation at two electrodes. The magnitude and direction of the resulting electric field are dependent on the conductivity conditions in the rock. The measurements are performed by means of a further pair of electrodes; for this purpose, the difference between the potentials at the electrodes is determined. The input electrodes ( $C_1$ ,  $C_2$ ) and the output electrodes ( $P_1$ ,  $P_2$ ) are arranged as single dipoles (Figure 3-1). For a complete data set, the position of the input dipole is fixed and the output dipole is moved around the area to be investigated. Afterwards, the input dipole is moved to another position, and the measurements are repeated. From the measured potential difference (voltage) and the imposed current, the value of the electrical resistivity is obtained in accordance with Ohm's law, with due consideration of the relative position of the four electrodes with respect to one another.

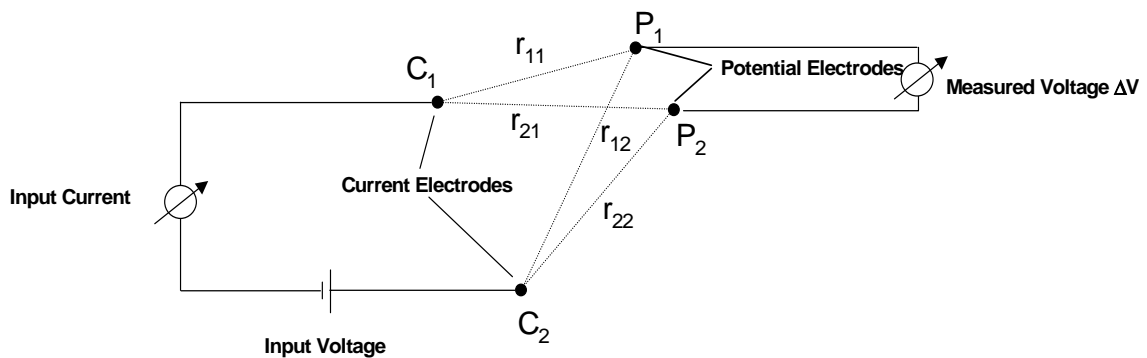


**Figure 3-1** Principle configuration of a dipole-dipole measurement

$$\Delta V = \frac{1}{4\pi} I\rho \left( \frac{1}{r_{11}} - \frac{1}{r_{12}} - \frac{1}{r_{21}} + \frac{1}{r_{22}} \right) \quad (17)$$

Although methods of direct current geoelectrics are employed for the evaluation of geoelectric measurements, modern resistivity meters use low-frequency alternating current rather than direct current. The reasons are:

- Direct current would cause electrolytic polarization, i. e. build-up of ions around the electrodes. This is prevented by periodic reversal of the current.
- Telluric currents, i. e. natural electric currents in the ground, can be accounted for in the measurements when the current is reversed and the measurement results are averaged, since the telluric currents do not change their polarity.

### **3.2 Measurement Evaluation**

Measurement evaluation is performed by inverse finite element modelling. Starting with a usually homogeneous model, the expected vector of apparent resistivities for the set of measurement configurations is calculated and compared to the actually measured apparent resistivities. The model is then iteratively improved in order to minimize the deviations between calculated and measured values.

The finite element mesh has to be adapted to the electrode array. The maximum attainable resolution is half the electrode spacing; this is the minimum side length of the finite elements. On the other hand, the attainable resolution has to be considered when designing the electrode array. Half the electrode spacing is the theoretically maximum attainable resolution – if an electrode was placed at every second grid point of the mesh, the inversion result would be definite. In reality, such a high number of electrodes and related measurement configurations is not feasible. Consequently, there are areas further away from electrodes where resolution and accuracy decrease. Therefore, scoping calculations are necessary before installing the electrodes in order to find out whether the expected effects can be detected (see chapter 6).

For the evaluation of the measurements, GRS uses the commercial software package SensInv2D (Fechner, 2001) which allows a two-dimensional inversion of the measured apparent resistivity data. Several strategies for applying iterative improvements to the resistivity model are implemented in this software. GRS employs the **multiplicative simultaneous inversion reconstruction technique** (MSIRT; Kemna, 1995) which is controlled by the sensitivity distribution of the model.

Each single measurement configuration gives a so-called sensitivity distribution, which is the matrix of partial derivatives of measured impedance against resistivity. Thus, the sensitivity at a special finite element describes how sensitive the result of this single measurement is to changes in resistivity. The cumulative sensitivity is the sum of the sensitivity matrices of all single measurements, thus describing where a resistivity change has a high influence on the overall results, and where not. Cumulative sensitivity is a measure for accuracy and reliability of the resistivity results. It is usually highest near the electrodes and lowest farther away.

Evaluation of the geoelectric measurements leads to a two-dimensional resistivity distribution that is supposed to be close to the true resistivity field. In order to interpret this resistivity distribution in terms of water content distribution, laboratory measurements have to be performed at defined saturation conditions (see chapter 5). Using the results of the laboratory calibrations, information on water content can be derived from the resistivity distribution.

### **3.3 Measurement System**

All geoelectric systems employed by GRS use low-frequency alternating current. Typically, 2 to 5 current cycles are injected during a single measurement. The period of a cycle is usually between 5 and 10 seconds. Such low frequencies are necessary in order to be able to treat the measurements as direct current geoelectrics; higher frequencies may result in phase differences between injected current and measured voltage. The injected current is in the range between 1 and 200 mA.

RESECS is a PC-controlled DC-resistivity monitoring system for high resolution tomography and other geoelectric applications. The RESECS measuring program runs under MS-Windows98. Up to 240 electrodes are separately addressable by unique decoder addresses. Any pair of electrodes might be selected as current injector. Up to six other pairs of electrodes might serve as potential electrodes for simultaneous geoelectrical measurements (six channel operation). The software controlled fast switching of electrodes results in a high data acquisition rate - up to a few thousands data points per hour.

Features of the stand-alone system are its flexible usage and its convenience in creating geoelectrical standard configurations (Wenner, Schlumberger, Dipole-Dipole etc.) as well as user-defined configurations for multi channel applications. All measuring parameter input is menu-driven.

In measuring mode RESECS automatically selects all programmed electrode configurations. It optimizes preamplification, corrects self potentials and yields DC-resistivity ( $\rho$ , U, I) as well as IP-values (phaseshift, chargeability). For standard configurations pseudosections and pseudodepth slices are displayed simultaneously. Current injection and its resulting potential differences are displayed online and can be stored on harddisk for later processing.

### **3.3.1 Hardware Components**

All system components are integrated in a 24 height units (HU) 19"-enclosure. The protection rating of the enclosure is IP54. The system is mounted on 4 twin swivel castors.

The front panel and rear panel of the system are illustrated in Figure 3-2 and Figure 3-3, respectively.

The RESECS resistivity meter essentially consists of the following components:

- Resistivity meter and embedded PC
- Injection voltage supply
- Electrode decoder array
- Uninterruptable power supply

### **3.3.2 Resistivity Meter and Embedded PC**

The resistivity meter and the embedded PC are mounted in a 19"-chassis. It is internally connected to the other components of the system.

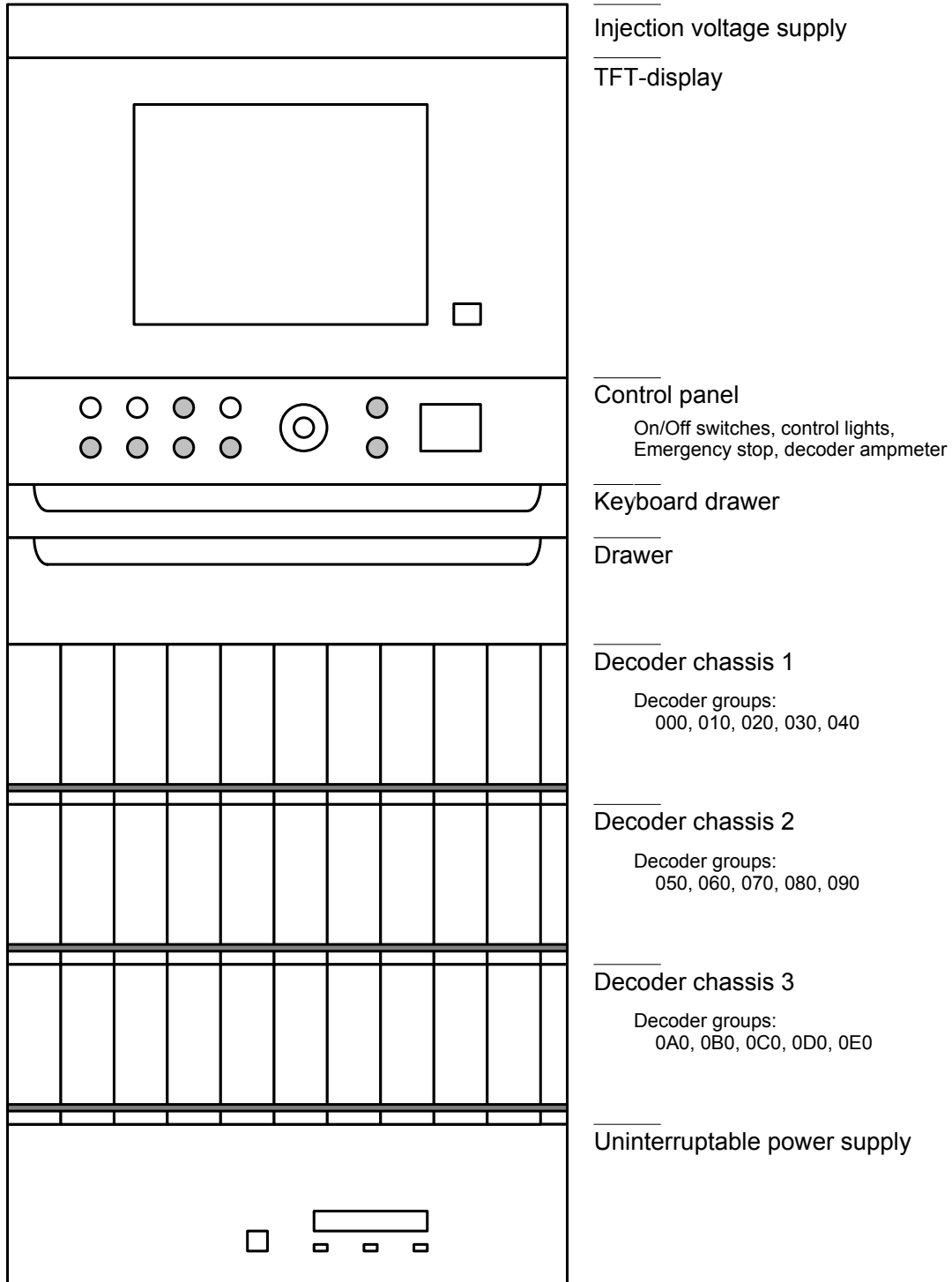


**Figure 3-2** Front view of RESECS measuring system

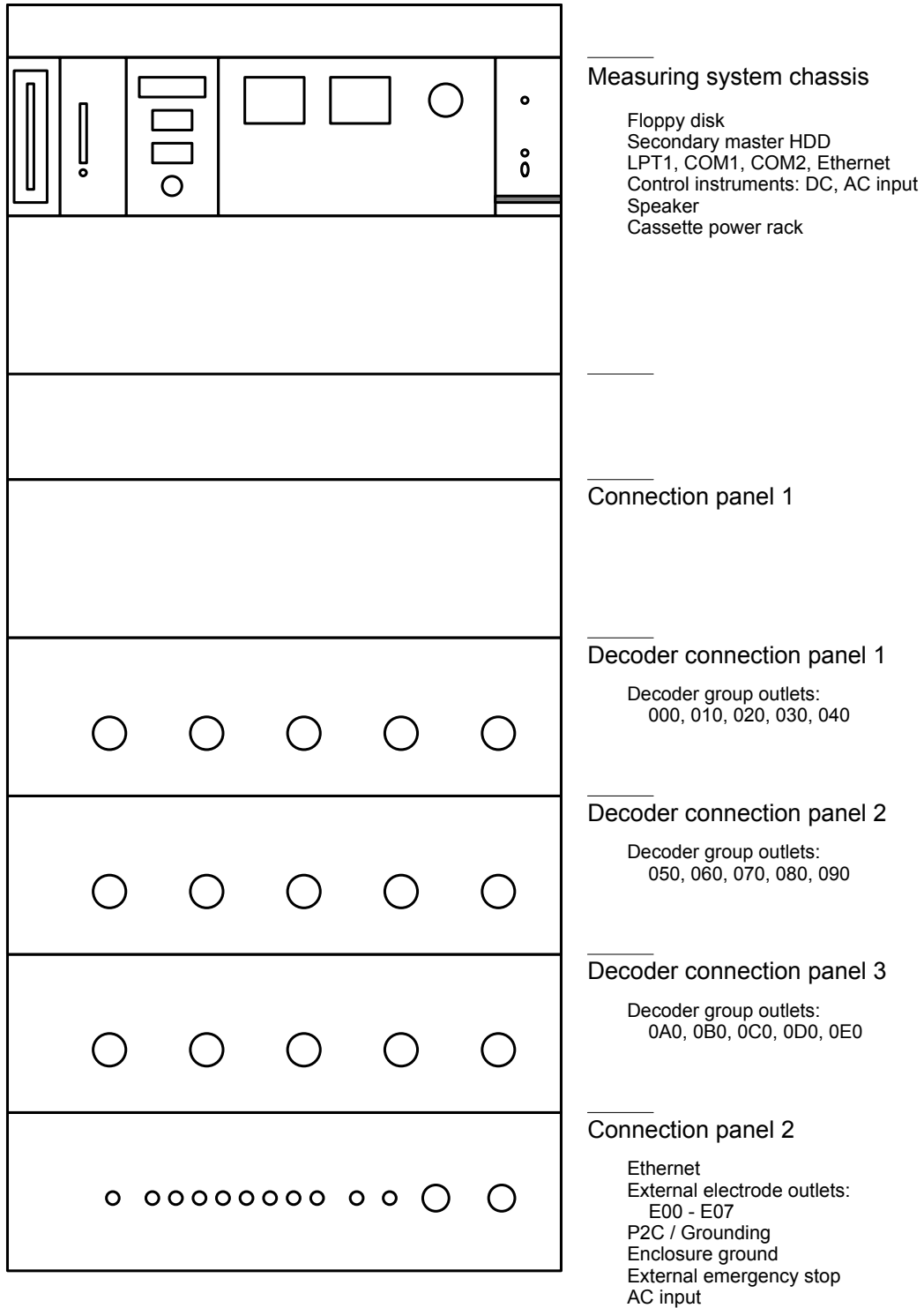


**Figure 3-3** Rear view of RESECS measuring system

The resistivity meter is controlled by the embedded PC. Up to six potential differences are measured simultaneously. Each analog input signal (injection current, potential differences) is supplied with a separate signal path. These signal paths are galvanically isolated from each other and from the embedded PC as well. Each one consists of high quality amplifiers (for impedance adaption, programmable gain setting and isolation), optocouplers and DC/DC converters for the separation of power supplies. Furthermore each signal path is supplied with a DC-accurate, tunable linear phase 5th order Bessel lowpass filter. The cutoff frequencies are software selectable. The AD-converter has a resolution of 16 bit and a conversion interval of 1 ms for each channel.

The injection voltage is switched using a full bridge consisting of high voltage transistors (FET). The switching timing is defined by software.

The electrode address code is created electronically by converting digital PC output to a serial function and address code.

The embedded PC (OCTAGON SYSTEMS PC510) is supplied with 33 MByte DRAM. The PC is set to the requirements of the measuring system. For detailed information refer to the PC510 users manual supplied on disk.

Further PC components are an ethernet card and two harddisk drives. The harddisks are formatted and partitioned. The user has access to the secondary master harddisk. The secondary master harddisk may only be removed from the system when the system is turned off.

### **3.3.3 Injection Voltage Supply**

The voltage supply, Xantrex XFR 600-2, serves as voltage supply for the injection current. This injection voltage source provides a maximum voltage of 600 V and a maximum current of 2 A. The voltage source is controlled by a serial PC interface (COM3). The switches on the rear panel of the voltage source are set to RESECS software requirements. For security reasons the output voltage is limited by software to 60 V in automatic monitoring measuring mode. In manual measuring mode the operator has full control over the output voltage.

### 3.3.4 Electrode Decoder Array

Electrode decoders are electronic circuits used for switching relays to the measuring lines C<sub>1</sub>, C<sub>2</sub>, P<sub>1</sub> or P<sub>2</sub>. Each decoder has a unique address and four different functions. Decoders are supplied in groups of 16. They are denoted with hexadecimal numbers. The lowest digit defines the decoder number within a decoder group. The second digit defines the group number. The highest digit is reserved for internal use.

Example of DID's (decoder identification)

000 - first decoder of first group

03A - tenth decoder of 4th group

0E1 - second decoder of 15th group

The system has a total number of 240 addressable electrode decoders.

The 18 pin electrode connectors at the rear panel of the system collect the outlets for one decoder group each. The decoders are connected to the pins in alphabetical order. They are denoted by the first decoder of the specified group. The pins labeled T and U are left unconnected.

Each 19" chassis contains 5 groups of decoders. A channel selector switch is located at the rear panel of the chassis. Remove the side cover of the enclosure to select the measuring channel for each group. As default setting, all groups are set to measuring channel 0. The hardware channel selection must be in accordance with software channel selection.

Activating and deactivating of electrode decoders is controlled by the measuring software. All decoders included in a measuring cycle are selected before the measurement and deselected before the next one. Only those decoders used for the next measuring cycle with the same function will not be deselected.

The supply voltage for the decoders is generated within the RESECS system.

It is galvanically isolated from other parts of the system. The decoder and relay supply current is displayed on the ampere-meter on the front of the system.

### **3.3.5 Uninterruptable Power Supply**

The system is supplied with an uninterruptable power supply, Knuerr UPS Modul NP 2000c. The purpose of the UPS is to provide power to the entire measuring system for at least 60 minutes in the event of voltage breakdown or power failure. It is connected to the PC by a serial interface (COM2) and is able to monitor malfunctions of the supply voltage.

### **3.3.6 Measuring Procedure**

The RESECS measuring software runs under MSWindows98. All input of measuring parameters is menu-driven. For detailed information refer to the RESECS software manual. The systems offers the possibility to create standard configurations like Wenner, Schlumberger, Dipole-Dipole as well as user defined configurations.

User defined configurations enable multi channel measurements. Up to six potential differences can be recorded simultaneously. These measurements require an user defined ASCII input file.

After creating a standard master project or an user defined master project all measurements can be controlled manually or automatically.

In monitoring mode the software creates copies of the master project and executes these daughter projects automatically. RESECS offers the opportunity to choose between different monitoring modi like start time controlled, interval controlled, number of cycle controlled or any combination of them. All measured values are stored on harddisk.

In the monitoring mode the voltage across the current electrodes is limited by software to 60 V for security reasons.

A typical screen display of the measuring software is illustrated in Figure 3-4.

At the top of the screen the menu items and main control button bar are displayed. Furthermore, the data window, a scope window, the pseudoarea plot, and the pseudosection are activated.

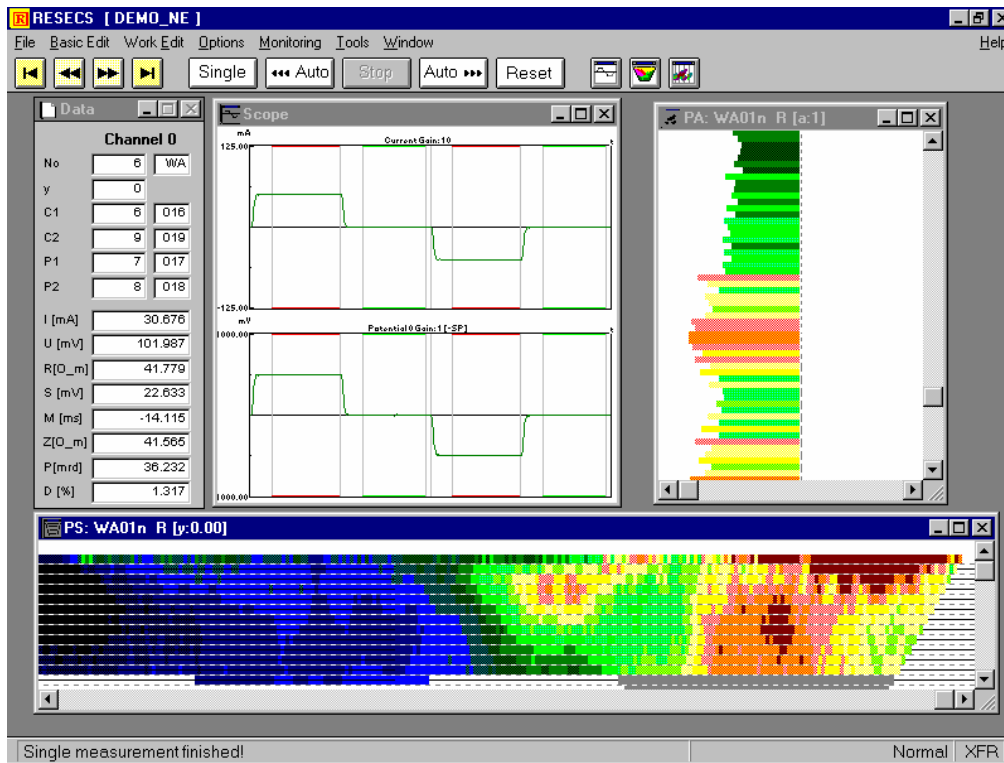


**Figure 3-4** Screen display of RESECS measuring software

## 4 Measuring Arrays in the Prototype Repository

The geoelectric in-situ measurements comprise monitoring of the backfill, the buffer, and the rock. An overview of the installed electrode arrays is shown in Figure 4-1.

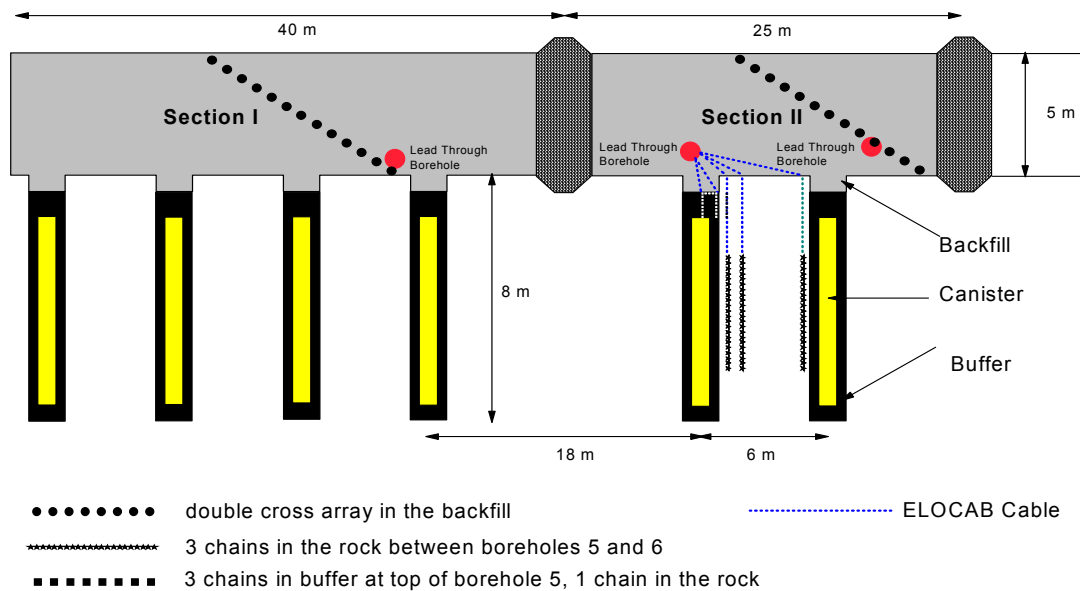


**Figure 4-1** Overview of electrode arrangements in the Prototype Repository

### 4.1 Backfill

Two double cross arrays consisting of 36 single electrodes each with a spacing of 0.5 m were installed on a 35° inclined backfill ramp above borehole 3 in section I (Figure 4-2) and above deposition borehole 6 in section II. These arrays are used to monitor the resistivity distribution in the backfill.

### 4.2 Buffer

The resistivity in the buffer at top of deposition borehole 5 is determined by geoelectric measurements involving one horizontal electrode chain installed on the surface of the buffer and three vertical electrode chains installed in the center of the buffer, about 10 cm from the borehole wall, and outside of the deposition borehole in the rock at 30 cm distance from the borehole wall (Figure 4-3 and Figure 4-4, respectively). The

spacing of electrodes is 0.1 m. The resistivity distribution is determined in the vertical plane containing the buffer electrodes.

### **4.3 Rock**

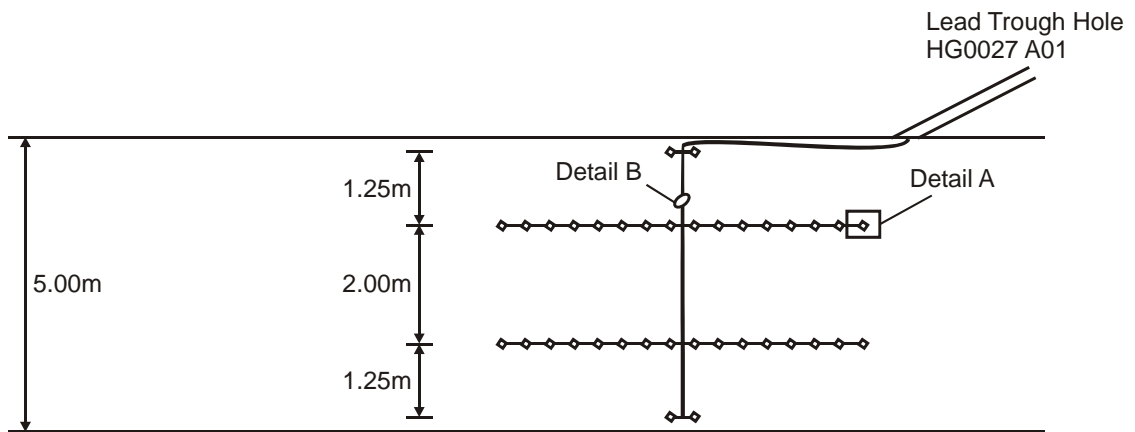
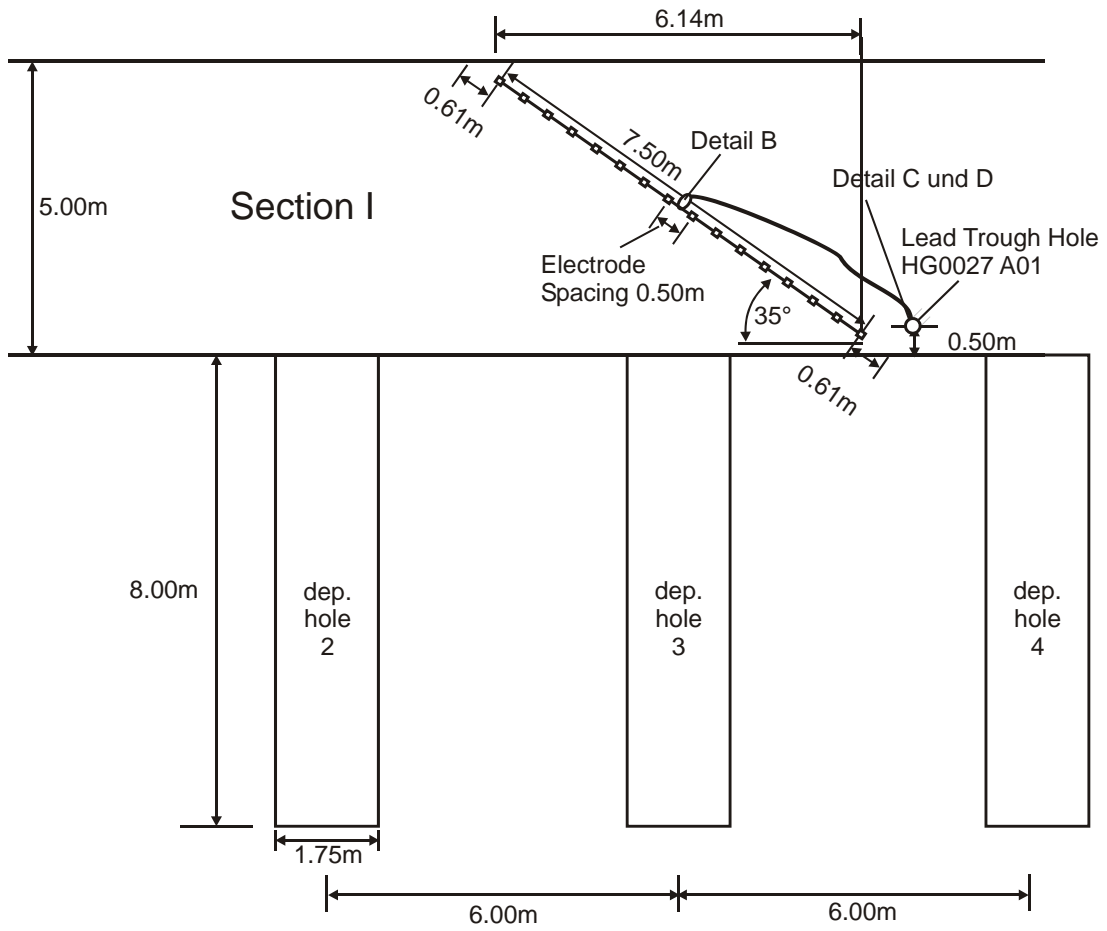
The resistivity distribution in the immediate vicinity of two of the deposition boreholes is monitored with electrode chains installed in three vertical boreholes in the rock between deposition boreholes 5 and 6 (Figure 4-4).

### **4.4 Electrodes and Electrode Chains**

Differently sized electrodes were manufactured for the different measurement arrays in the Prototype Repository. According to a recommendation of the Swedish Corrosion Institute the electrode material is a stainless steel type AISI 316 (also called SS2343).

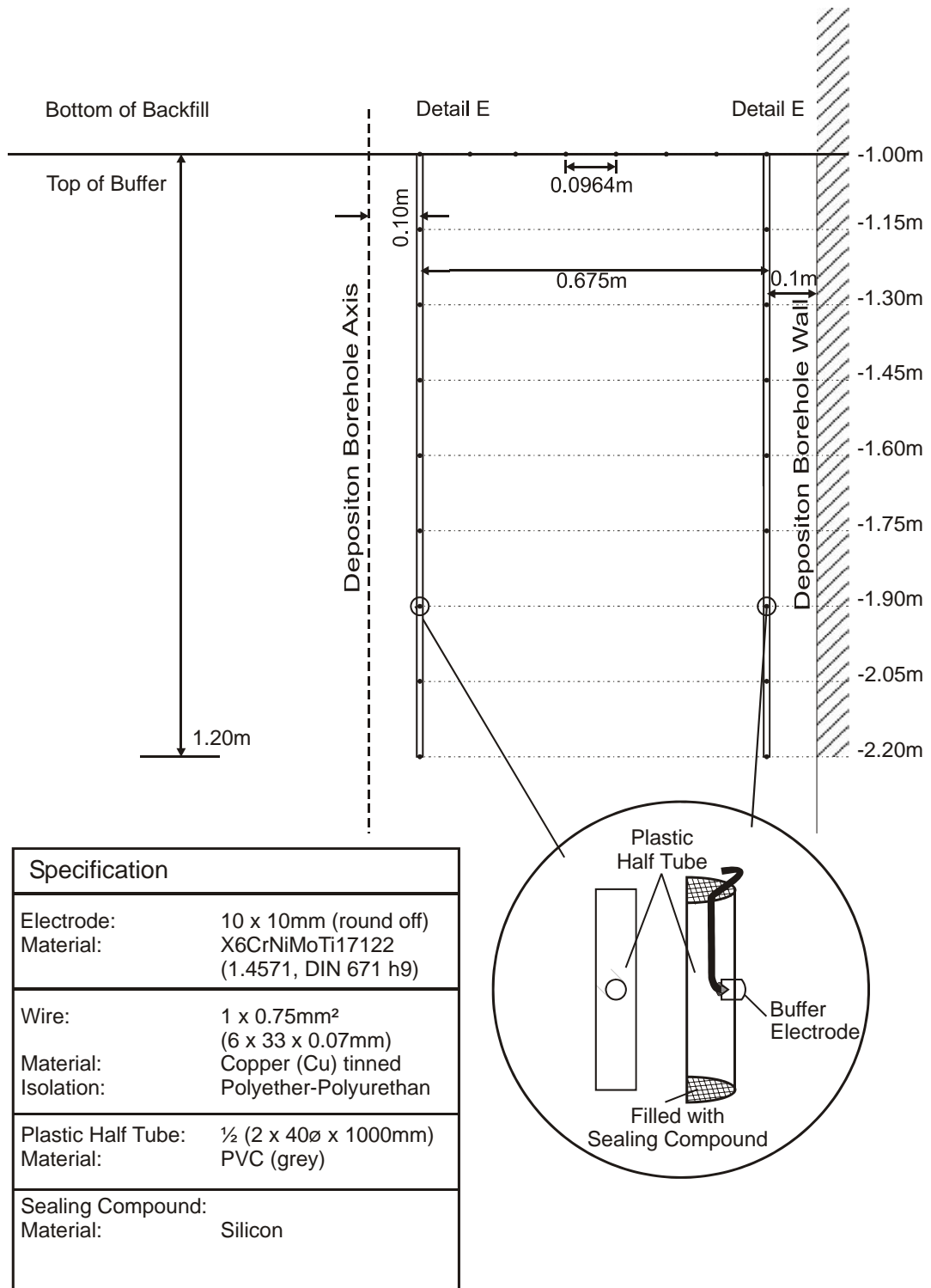
The electrodes were manufactured with diameters of 10 and 30 mm, respectively with an accuracy of  $\pm 0.1$  mm. Each electrode has a drillhole of 2 - 4 mm diameter and 5 -10 mm depth in its neck in which the measuring wire is fastened by silver soldering. The transition from the electrode to the cable is pasted with epoxy resin and sealed with a plastic sealing which is screwed onto the electrode's neck.

All electrode chains consist of an ELOCAB multiwire cable consisting of 37 insulated wires each filled with a swelling filler preventing migration of moisture inside the insulation sheathing (Figure 4-5). The cables are tight against a water pressure of 10 MPa perpendicular to the cable axis and 6 MPa along the cable axis.



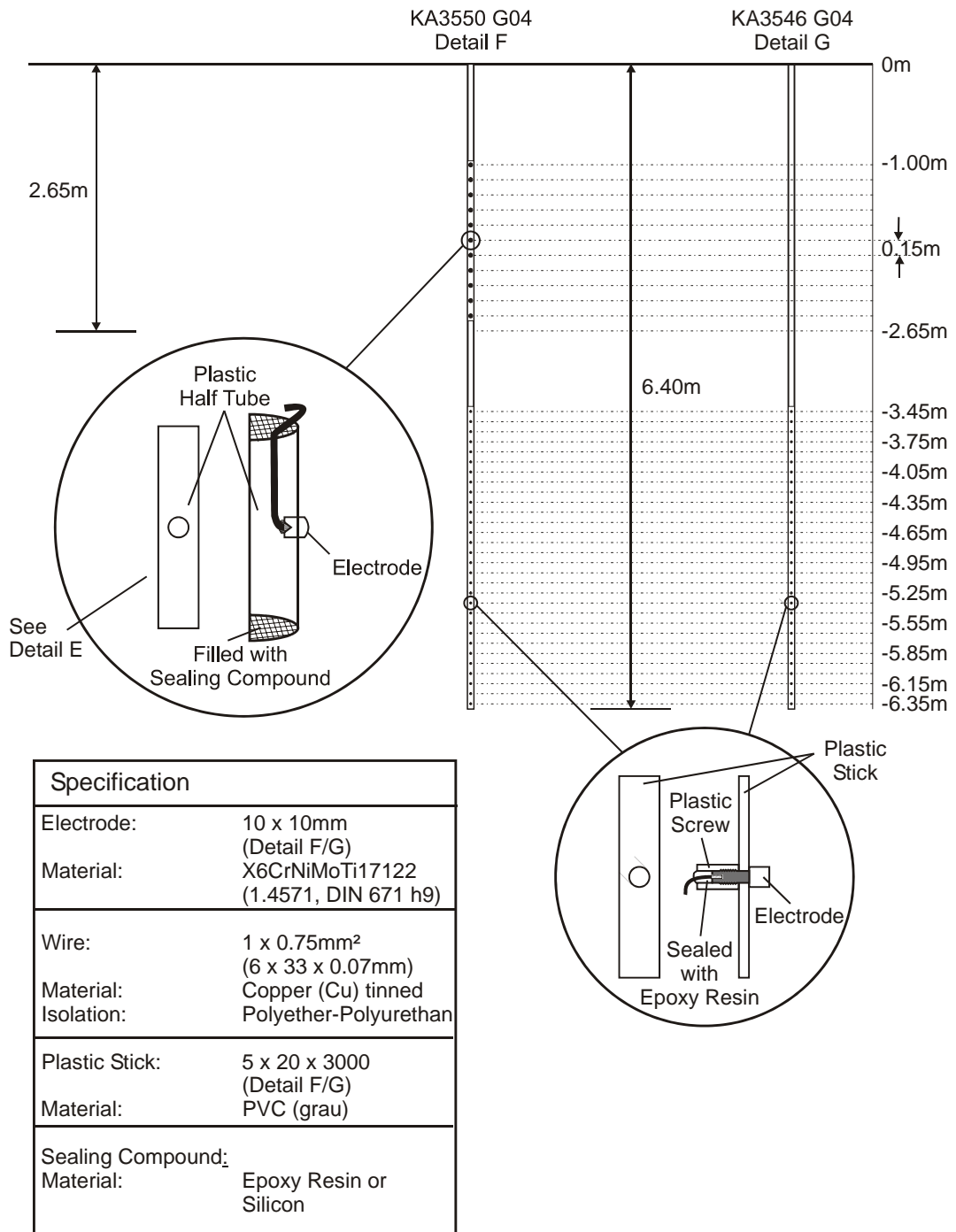
BACKFILL ELECTRODES SECTION 1.CDR

**Figure 4-2** Double cross electrode arrangement in the backfill



ELECTRODE DETAIL E.CDR

**Figure 4-3** Electrode chains at top of borehole 5



ELECTRODE DETAIL F-G VERS.01.CDR

**Figure 4-4** Design of electrode chains in the rock, showing the upper chain used for the buffer measurements and the lower chains for monitoring the rock

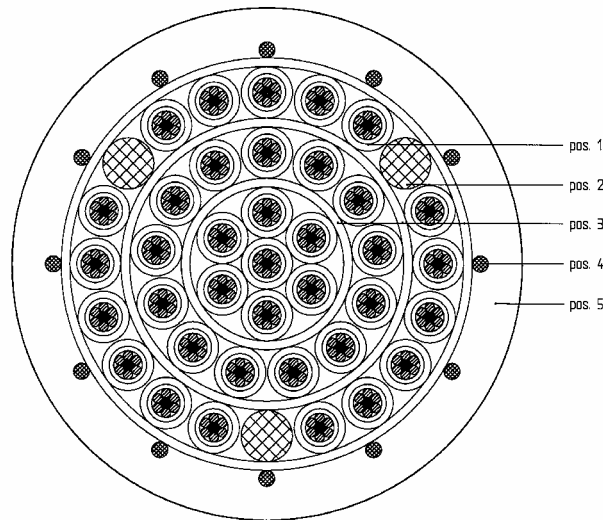
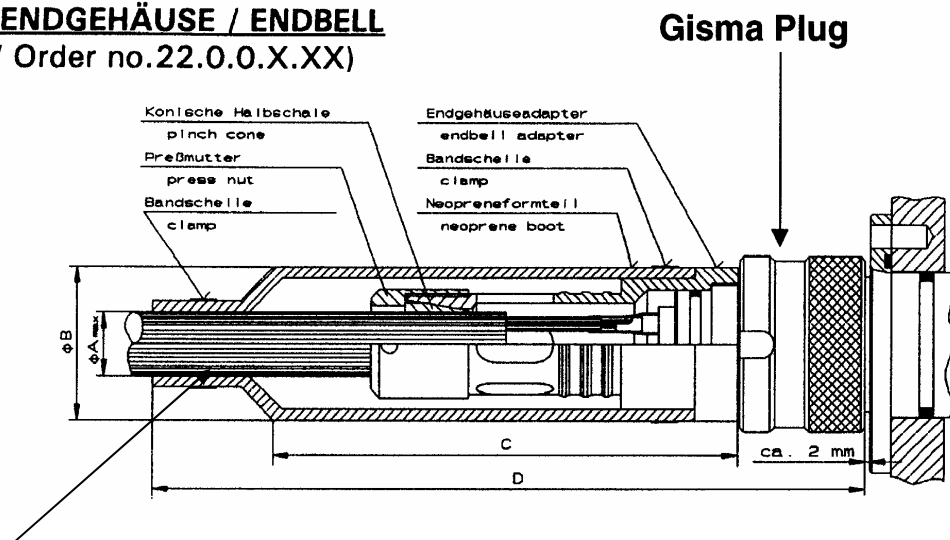


**Figure 4-5** Design of an ELOCAB-cable (diameter of multiwire cable: 27.5 mm, diameter of single wire: 2.7 mm)

The ELOCAB-cables are connected pressure tight to a GISMA-plug developed in submarine techniques (Figure 4-6). The GISMA-plugs are pressure tight, too up to water pressures of 10 MPa.

**VERGUSSENDGEHÄUSE / ENDBELL**  
(Best.Nr. / Order no.22.0.0.X.XX)



**ELOCAB Multiwire Cable ERK 7673 (37 pins)**

**Figure 4-6** GISMA-plug



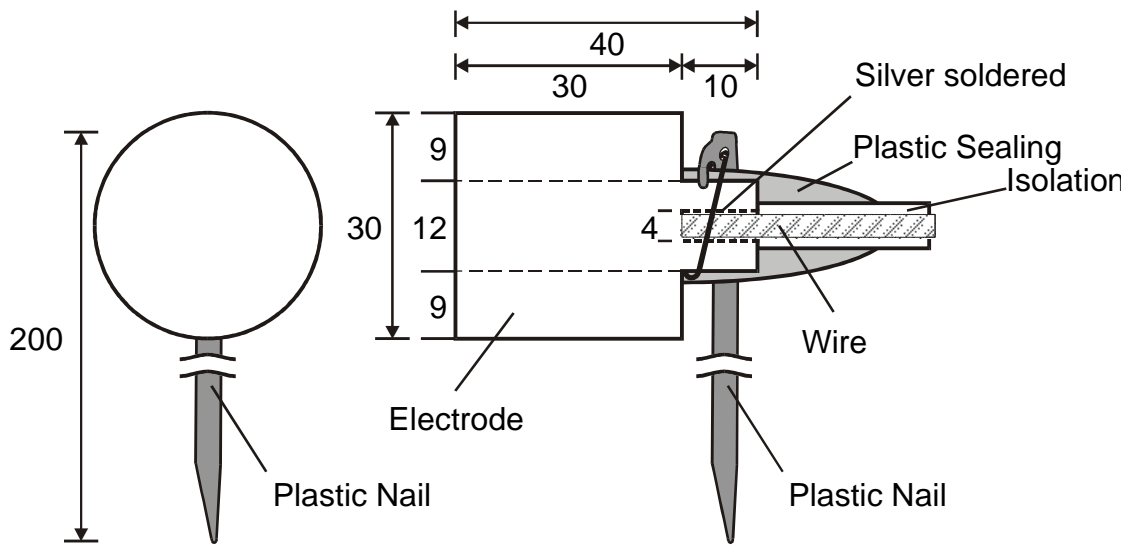
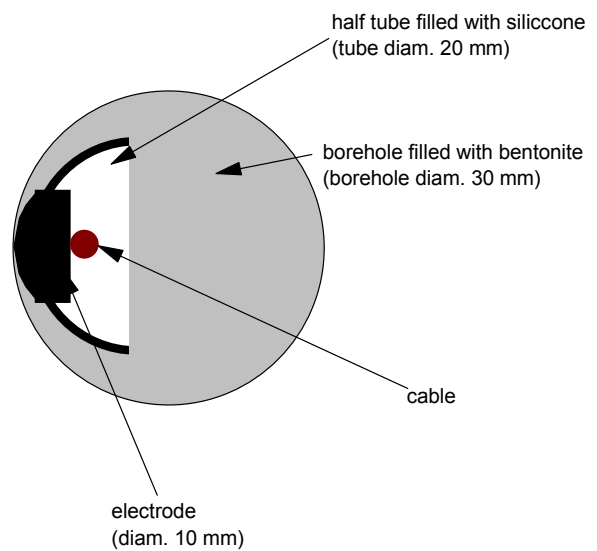


Figure 4-8 Design of a drift electrode



a) Test block of bentonite and mock up electrode chain



b) Horizontal cross section through buffer borehole

Figure 4-9 Design of electrode chain in the buffer

The electrode chains in the rock (Figure 4-4) consist also of an ELOCAB cable with the single wires soldered to 10 mm electrodes which are fixed to a plastic stick which was lowered into the borehole in the rock. To get proper contact of the electrodes to the rock the boreholes were grouted with a special cement/crushed rock mixture. After installation in the borehole, the GISMA-plug of the cable was plugged into the respective GISMA socket in the drift wall.

## 5 Laboratory Calibration

In order to enable adequate interpretation of the in-situ measurements, calibrations were performed at GRS's geotechnical laboratory in Braunschweig.

The calibrations include the determination of the resistivity of compacted MX-80 powder and of original pre-compacted buffer material samples provided by SKB as well as of the drift backfill in dependence of the water content and of temperature.

Besides its dependence on the water content, the electric resistivity is also a function of salinity and composition of the pore solution. Since both may change as the solution penetrates the buffer and the backfill, investigations were performed in order to quantify this effect.

### 5.1 Resistivity of MX-80-Bentonite

#### 5.1.1 Samples

##### *Preparation of compacted MX-80 samples with defined water content*

For the preparation of the samples with different water contents, the MX-80 powder was moisturized with Äspö-solution as presented in Table 5-1.

**Table 5-1** Composition of the used Äspö-solution [mmol/l]

Na	K	Ca	Mg	Cl	SO <sub>4</sub>
79.67	0.25	17.06	3.33	113.92	3.40

After drying of the MX-80 powder in an oven at 105 °C over 24 h, the water content of the delivered MX-80 material was determined to 9.8 wt % and 10.04 wt %. Under consideration of this value, the total water content of the samples was obtained by adding an adequate amount of Äspö solution.

Subsequently, the moist powder was compacted in a specially constructed resistivity measurement cell (see Figure 5-1) to a dry density of 1.66 g/cm<sup>3</sup> which is considered a

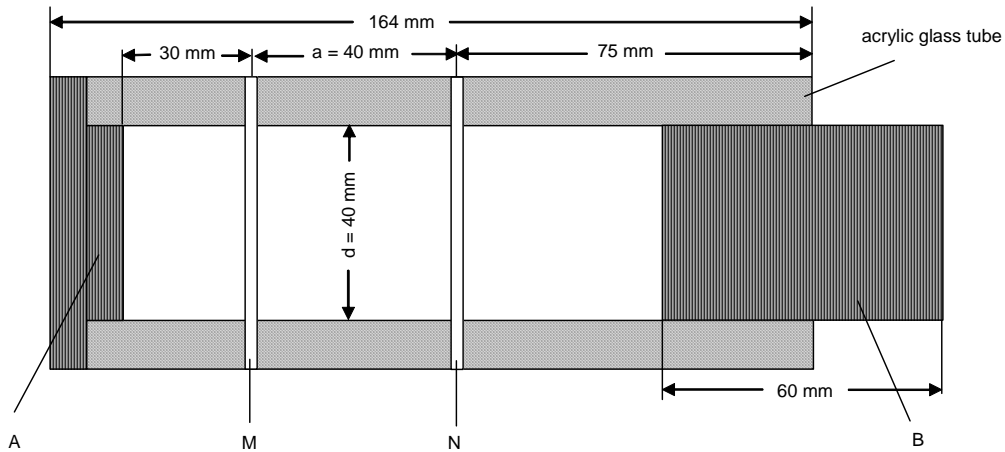


**Figure 5-1** Schematic view of the resistivity measurement cell for compacted MX-80 samples

representative value for the conditions at the top of a deposition borehole (Dahlström 1998). For each water content a new sample was produced. For the investigations on the influence of temperature, samples with a constant water content of 19.4 wt % related to the dry MX-80 were produced. For the determination at elevated temperatures the compacted MX-80 in the measuring cell was heated in an oven up to 35 °C and 70 °C.

The specifications of prepared samples and their water content are shown in Table 5-2.

#### ***Preparation of original Äspö MX-80 buffer samples***

Cylindrical samples were prepared from original bentonite bricks provided by SKB. These samples had a different initial water content of about 13 and 17 wt %, respectively. Three samples were prepared from the 13-wt %-material and marked as ÄSPÖ-PR-BFST 13/1 to 13/3 and three further samples from the 17-wt %-material marked as ÄSPÖ-PR-BFST 17/1 to 17/3.

The water content of the original bricks was determined on material remaining from sample preparation by drying in an oven at 105 °C over 24 h.

The size of the samples and their water content at time of investigation are summarized in Table 5-2.

**Table 5-2** Water content and size of the prepared MX-80 samples and of the original buffer samples

sample	water content	sample length	sample diameter
	wt %	mm	mm
compacted MX-80 samples			
MX-80/1	10.9	100.0	40
MX-80/2	16.5	100.0	40
MX-80/3	22	96.1	40
MX-80/3a	22	95.0	40
MX-80/4	27.5	86.4	40
MX-80/5	32.9	87.1	40
MX-80/6 22 °C	19.4	102.0	40.2
MX-80/6 35 °C	19.4	102.0	40.2
MX-80/6 70 °C	19.4	102.5	40.2
MX-80/7 22 °C	19.4	101.8	40.2
MX-80/7 35 °C	19.4	102.2	40.2
MX-80/7 70 °C	19.4	102.5	40.2
samples from original Äspö buffer material			
ÄSPÖ-PR-BFST 13/1	12.5	97	50
ÄSPÖ-PR-BFST 13/2	11.9	97	50
ÄSPÖ-PR-BFST 13/3	11.7	97	50
ÄSPÖ-PR-BFST 17/1	14.3	97	50
ÄSPÖ-PR-BFST 17/2	14.1	97	50
ÄSPÖ-PR-BFST 17/3	14.1	91	50

### 5.1.2 Measurement and Evaluation

The resistivities of the compacted MX-80 samples with varying water content were measured at ambient temperature in the specially constructed cell shown in . At the ends of a plastic tube, the current electrodes A and B were installed. Since the samples varied in length, the electrode B was moveable. Two brass rings (voltage electrodes M and N) were inserted in the acrylic glass tube.

For the resistivity measurement of the samples prepared from the original bricks, the cylindrical samples were set between two metal plates A and B (Figure 5-2). A potential difference U was measured at the electrodes M and N which had been installed at the surface of the sample.

The resistivity of the samples was determined by using the four-point method. The current I was conducted at the current electrodes A and B of both sides of the sample and the voltage drop U was measured at the voltage electrodes M and N. According to (Schick et al. 1973) and (Kull et al. 2001), the resistivity was calculated by:

$$\rho = \frac{U \cdot A}{I \cdot a} \quad (18)$$

with:

$\rho$  = resistivity [ $\Omega\text{m}$ ]

U = electrical voltage [V]

I = current [A]

a = distance of the voltage electrodes M and N

A = cross section of the sample [ $\text{m}^2$ ]

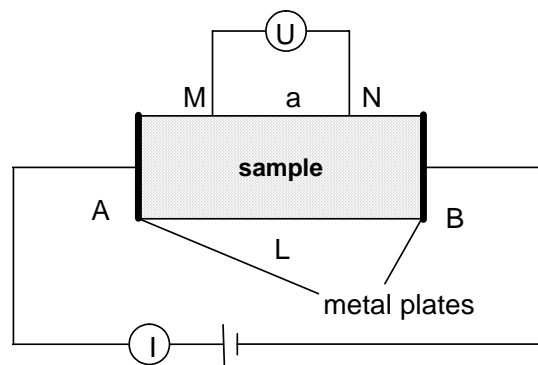


**Figure 5-2** Schematic experiment layout for the determination of sample resistivity (4-point method)

### 5.1.3 Results

The results show that the resistivities of the compacted MX-80 samples at ambient temperature decrease with increasing water content (Figure 5-3). The resistivities range between 34.5 and 1.6  $\Omega\text{m}$ . The water content varies between 10.9 and 32.9 wt %. The highest resistivity (34.5  $\Omega\text{m}$ ) was measured at the lowest water content of 10.9 wt %. A small increase of the water content to 16.5 wt % already leads to a significant decrease of resistivity (6.8  $\Omega\text{m}$ ). At higher water contents above 22 wt % up to 32.9 wt %, the change of resistivity is insignificant.

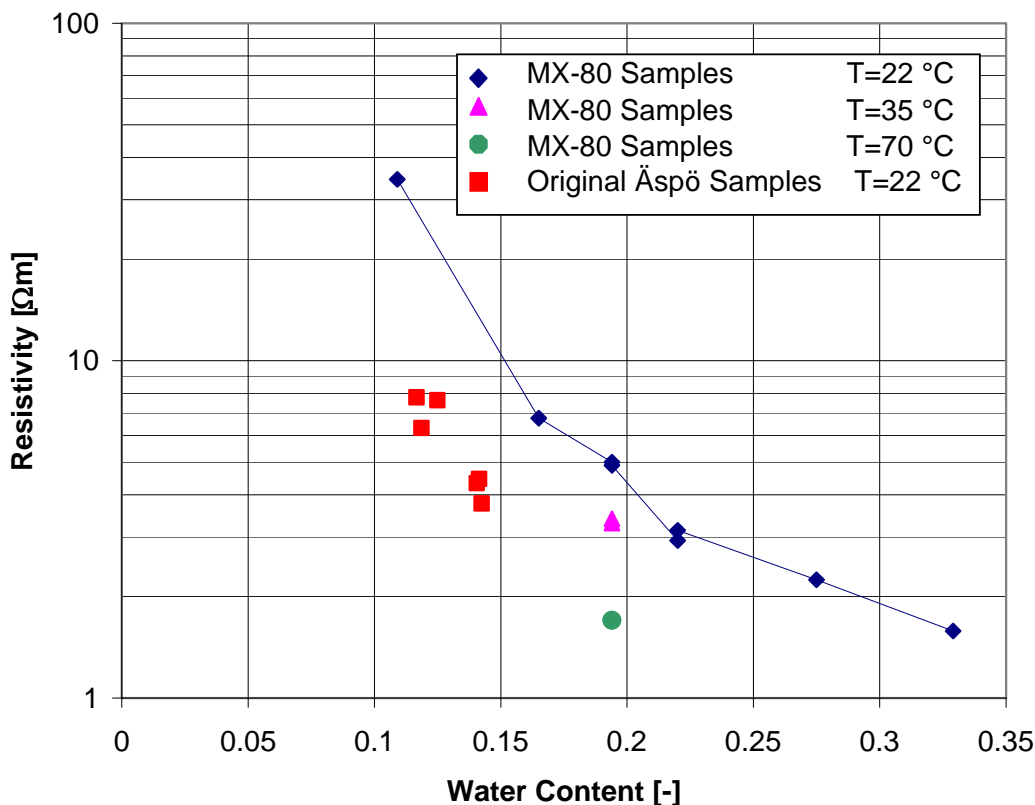


**Figure 5-3** Resistivity of compacted MX-80 samples and original ÄSPÖ buffer material as a function of the water content

At elevated temperatures the resistivities of the samples with a water content of 19.4 wt % decrease with increasing temperature. The resistivities at 35 °C are about 3.4 Ωm and 1.7 Ωm at 70 °C, respectively. Probably, this result can be explained by the temperature dependence of the solution, because the conductivity of most electrolyte solutions increases with increasing temperature. But it can be caused by the temperature influence on the resistivity of the bentonite or the granite, too. For a better interpretation appropriate investigations are necessary.

The resistivities of the original buffer material range between 6.3 Ωm and 7.8 Ωm at water contents of about 12 and 13 wt % (samples ÄSPÖ-PR-BFST 13/1 to 13/3) and 3.8 Ωm and 4.5 Ωm at water contents of about 14 wt % (samples ÄSPÖ-PR-BFST 17/1 to 17/3). The resistivities are in the same range as those of the compacted MX-80 samples at comparable water contents. The water content and the corresponding resistivities are summarized in Table 5-3.

**Table 5-3** Summary of the water content and the resistivities of the compacted MX-80 samples and the original Äspö buffer material

MX-80 sample	temperature	water content	resistivity
	°C	wt %	Ωm
compacted MX-80 samples			
MX-80/1	22	10.9	34.5
MX-80/2	22	16.5	6.8
MX-80/3	22	22	2.9
MX-80/3a	22	22	3.1
MX-80/4	22	27.5	2.2
MX-80/5	22	32.9	1.6
MX-80/6	22	19.4	5.0
MX-80/7	22	19.4	4.9
MX-80/6	35	19.4	3.4
MX-80/7	35	19.4	3.3
MX-80/6	70	19.4	1.7
MX-80/7	70	19.4	1.7
samples from original Äspö buffer material			
ÄSPÖ-PR-BFST 13/1	22	12.5	7.6
ÄSPÖ-PR-BFST 13/2	22	11.9	6.3
ÄSPÖ-PR-BFST 13/3	22	11.7	7.8
ÄSPÖ-PR-BFST 17/1	22	14.3	3.8
ÄSPÖ-PR-BFST 17/2	22	14.1	4.5
ÄSPÖ-PR-BFST 17/3	22	14.1	4.3

The steep drop of resistivity at the lower water contents can be explained by a clay-typical interface conductivity which is due to additional cations held loosely in the diffuse part of the electrical double layer surrounding the clay particles (Serra 1984). Already a small amount of solution leads to formation of a double layer and causes the interface conductivity.

Because of the relatively small resistivity changes observed at higher saturation it seems obvious that the interface conductivity is the predominant part of the conductivity in the MX-80 bentonite.

The total conductivity is a sum of the conductivity of the free solution in the pore space and the interface conductivity. According to Schopper (1982), the conductivity of a solution saturated porous rock can be described by

$$\sigma_0 = \frac{1}{F} \sigma_w + \sigma_{q0} \quad (19)$$

with  $\sigma_0$  being the total conductivity of the fully saturated rock,  $F$  the formation factor,  $\sigma_w$  the electrolytic solution conductivity, and  $\sigma_{q0}$  the interface conductivity.

## 5.2 Drift Backfill

### 5.2.1 Samples

For reasons of comparison, the backfill samples were prepared to represent the backfill conditions right after installation. These are the design density of 1.7 g/cm<sup>3</sup> and the initial water content of 12 wt % which means a dry density of the backfill of 1.5 g/cm<sup>3</sup>.

The initial water content of both the crushed rock and the Milos bentonite were determined according to DIN 18121-1 by drying in an oven over 90 hours at 105 °C and subsequent measurement of the weight loss. According to the measurements, the crushed rock has an initial water content of 1.20 wt % and the Milos bentonite of 13.09 wt %.

Samples of differently moisturized backfill were prepared by first mixing pure crushed rock and Milos bentonite as delivered by SKB and subsequent spraying of predetermined amounts of Äspö water (compare ) into the material until the desired total water content was achieved. Seven samples as shown in Table 5-4 were prepared.

**Table 5-4** Water content and achieved dry density of backfill samples

Backfill sample	Water content wt %	achieved dry density g/cm <sup>3</sup>
Sample 1	12	1.33
Sample 2	13	1.53
Sample 3	15	1.45
Sample 4	18	1.48
Sample 5	21	1.50
Sample 6	25	1.51
Sample 7	33	1.27

Figure 5-4 shows emplacement of the moisturized material into the specially designed and fabricated measurement cell and Figure 5-5 shows a four-point-measurement set-up. All samples were manually compacted as far as possible to achieve the dry density of  $1.5 \text{ g/cm}^3$ . Especially at the highest water content of 33 wt % it was impossible to achieve the dry density of  $1.5 \text{ g/cm}^3$  because the material was very sticky. Regarding the determination of electrical conductivity or resistivity, however, all samples were considered acceptable.

### 5.2.2 Results

For different water contents, the resistivity measurements of the compacted crushed rock/Milos bentonite samples were performed at 22 °C 35 °C and 50 °C. The results are presented in Figure 5-6. All three resistivity curves show a decrease in resistivity with increasing water content. The resistivities measured at 22 °C range between  $16.3 \text{ }\Omega\text{m}$  and  $1.9 \text{ }\Omega\text{m}$  at water contents of 12 wt % and 33 wt %. The resistivities measured at 35 °C are lower and show values between  $9.7 \text{ }\Omega\text{m}$  and  $1.7 \text{ }\Omega\text{m}$  at comparable water contents. At 50 °C the resistivities vary between  $9.5 \text{ }\Omega\text{m}$  and  $1.3 \text{ }\Omega\text{m}$  and show the lowest values. These results are in good agreement with the results obtained on compacted MX-80 samples and original ÄSPÖ MX-80 buffer samples and show the same characteristic steep resistivity decrease at lower water contents. Because of the similar behaviour of buffer and backfill it is concluded in addition, that the bentonite governs the resistivity behaviour of the backfill.

The resistivities at the higher temperatures (50 °C and 35 °C) are lower than the values measured at 22 °C. This is explained by the temperature dependence of the pore solution because the conductivity of most electrolyte solutions increases with increasing temperature. But it can be caused by the temperature influence of the resistivity of the bentonite or the rock material, too. For a better interpretation, appropriate investigations would be necessary.



**Figure 5-4** Emplacement of moistured backfill into measurement cell for determination of material resistivity



**Figure 5-5** Measurement set-up for determination of backfill resistivity

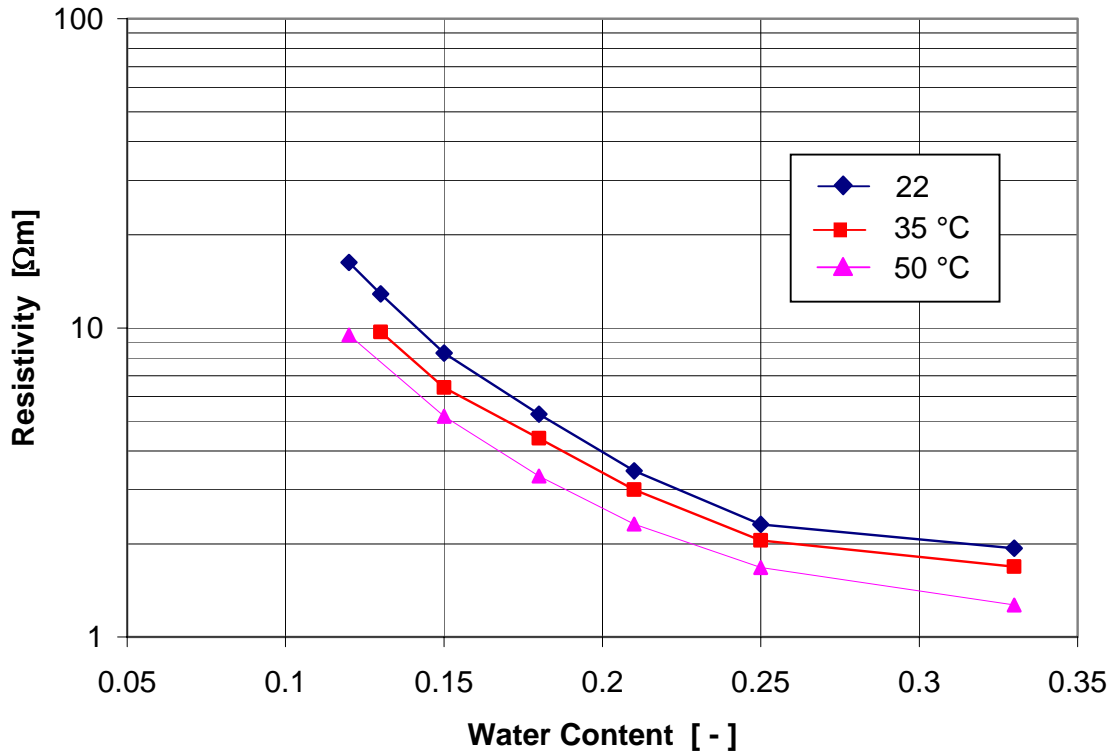


**Figure 5-6** Resistivity of compacted backfill samples versus water content

### 5.3 Rock

Regarding the granite rock, calibration measurements on rock samples were performed. Because a temperature increase in the rock around the boreholes are assumed, laboratory calibrations were carried out in order to determine the relation between resistivity and water content in dependence of the temperature.

The investigations were performed on fifteen cylindrical samples. The diameter of the samples was approx. 35.3 mm and the length approx. 79 mm. In order to remove irritating crystallized salts and electrolytes from the pore space by diffusion and to ensure therefore a defined starting point the samples were diluted with water first and dried at 105 °C afterwards.

For saturation with the Äspö-specific solution (for composition see Table 5-1), first the samples were evacuated in an exsiccator (Figure 5-7) and then the ÄSPÖ-specific solution was added. The conductivity of the Äspö solution was 2.62 mS/cm (T=25 °C). The samples were stored at these conditions of about four weeks.



**Figure 5-7** Exsiccator with granite rock samples

For the investigations at the three temperature steps of ambient temperature, 35 °C, and 70 °C, the samples were distributed into three parts. At each temperature the saturation was changed by drying at ambient air conditions, with vacuum or at elevated temperatures.

In contrary to the measurements at buffer and drift backfill, the resistivities of the rock samples were determined using the 2-point method. Due to the very high resistivities at the dry stage of the rock, at the 4-point method the internal resistance of the voltmeter leads to an incorrect measurement of the voltage.

The measurement of the electric resistivity was performed using the two-point method by applying a known voltage to the planes of the sample and measuring the resulting current (Figure 5-8 and Figure 5-9). To achieve a good coupling between the metal plates and the sample, the planes of the sample were coated by highly conductive silver paint (Figure 5-10).

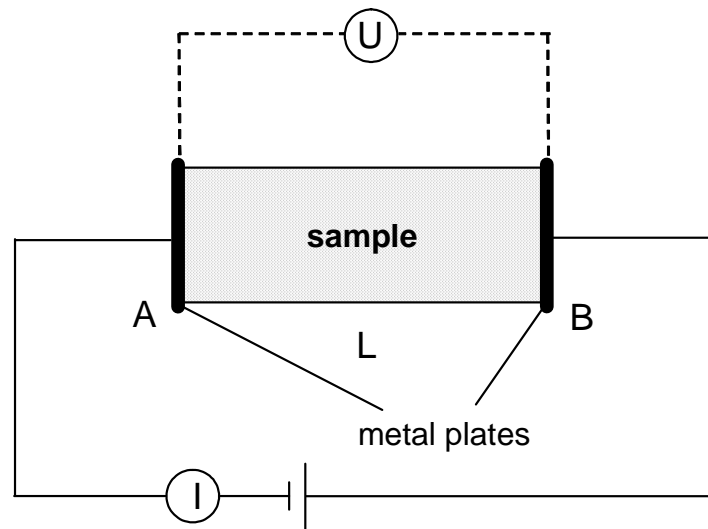


**Figure 5-8** Schematic of the 2-point arrangement for the determination of the resistivity

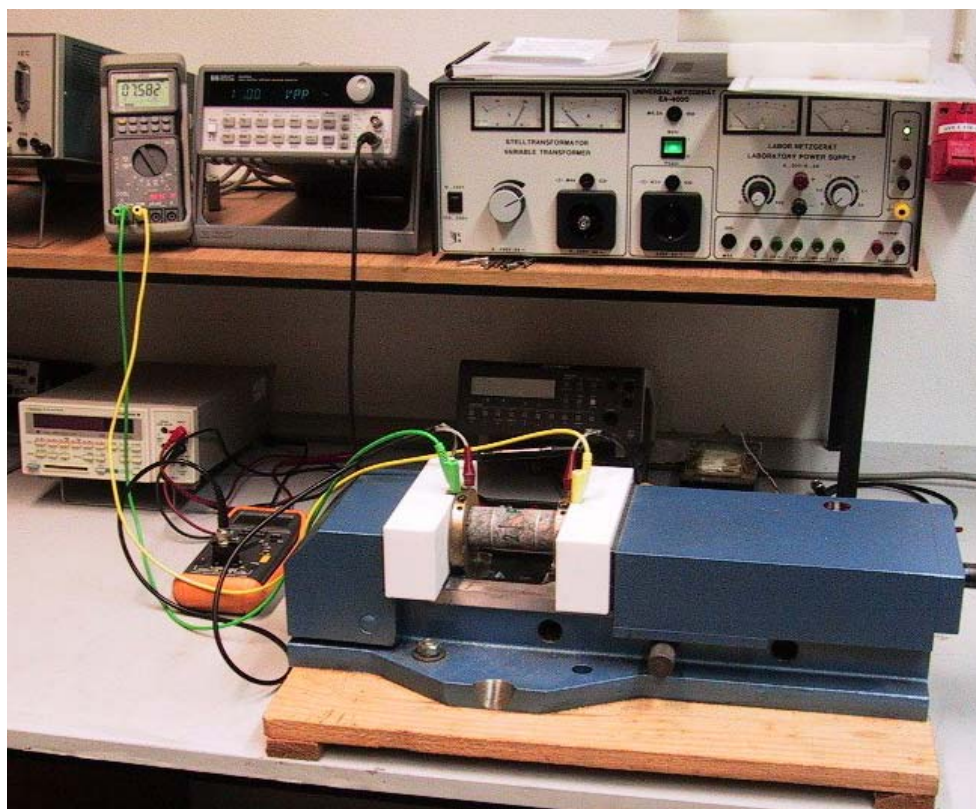


**Figure 5-9** Measurement set-up for determination of clay rock resistivity



**Figure 5-10** Sample coated with conductivity silver lacquer

The resistivity was calculated by:

$$\rho = \frac{U \cdot A}{I \cdot L}$$

with:

$\rho$	resistivity, $\Omega\text{m}$
$U$	electrical potential, V
$I$	current, A
$L$	sample length, m
$A$	cross section, $\text{m}^2$

Due to the very low porosities of the granite samples, a defined desaturation was difficult. The porosities, calculated from the mass of water at full saturation ranged between 0.32 to 1.25 %.

The results of the resistivity measurements show that the resistivities of the rock samples increased with decreasing saturation. The resistivities ranged between 2218  $\Omega\text{m}$  up to 10,588  $\Omega\text{m}$  at full saturation and between 105,900  $\Omega\text{m}$  up to 530,294  $\Omega\text{m}$  at lowest saturation. The results are presented in Figure 5-11.

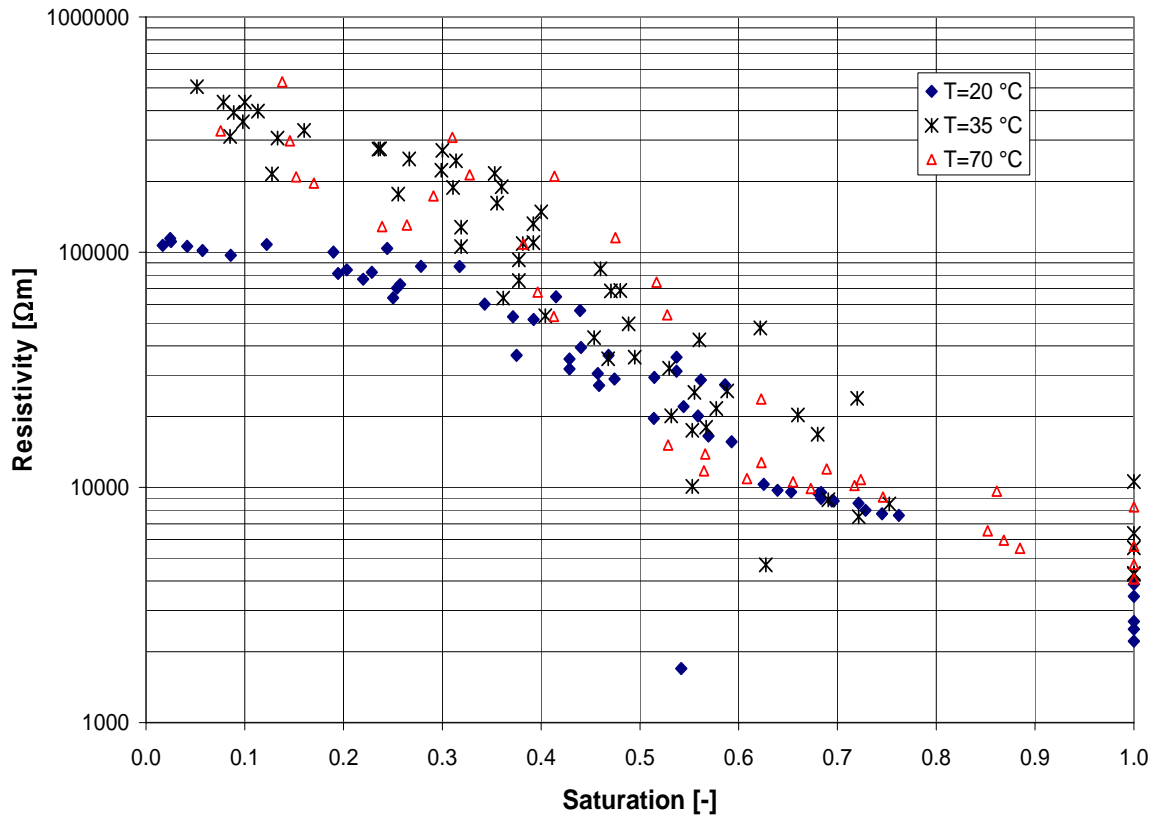


**Figure 5-11** Resistivity of granite at different saturations and temperatures

At saturations between 20 % and full saturation, the influence of the temperature was not significant. Only at saturations below 20 % a difference between the resistivities at 20 °C and the elevated temperatures could be observed. At higher temperature, only a slight increase in the resistivity was measured. This observation is in contrary to the results of the investigations on backfill, where the resistivities were lower at higher temperatures. Normally the conductivity of most electrolyte solutions increases with increasing temperature. Due to the very small pore spaces of the granite, it is possible, that the temperature leads to a hindrance of the motion of the ions.

#### 5.4 Cementation Material

Three electrode chains will be installed in the rock boreholes between deposition boreholes 5 and 6. In order to get proper contact of the electrodes to the surrounding rock the boreholes are to be grouted with a cement. Most suitable is a cementation material which exhibits a similar resistivity as the fully saturated surrounding rock. In order to determine the best suited cementation material laboratory investigations were carried out using different granite dust-cement and sand-cement ratios with water and

an ÄSPÖ specific solution. The criterion for the decision was an acceptable resistivity and a mixture which was capable of being cast.

#### 5.4.1 Samples

For the investigations cylindrical samples were performed of different mixtures of cementation materials. The used components were granite dust, fine sand, Portland cement, water and an ÄSPÖ-specific solution, respectively. The diameter was about 4.8 cm and the length of the specimens ranged between 6.6 cm and 14.7 cm. In Table 5-5 the ratios of the different mixtures are summarized.

**Table 5-5** Investigated mixtures of cementation materials

		<b>water/cement ratio (W-C ratio)</b>	<b>ÄSPÖ- solution/cement ratio (ÄS-C ratio)</b>
G-C -W	granite/cement= 6:1	1:2 1:1.33 2:1	- - -
S-C-W	sand/cement= 6:1	1:1.33 2:1	- -
G-C-ÄS	granite/cement= 4:1	-	1:0.67
S-C-ÄS	sand/cement= 4:1	-	1:0.67

To assure a better coupling of the electrodes with the samples the end surfaces were supplied with conductivity lacquer.

#### 5.4.2 Measurement and Evaluation

After setting of the cement, first measurements at the virgin state of the samples were performed. The samples produced with water (G-Z-W, S-Z-W), and one part of the samples produced with an ÄSPÖ-specific solution (G-C-ÄS, S-C-ÄS) were dried under ambient conditions. To simulate the wetness of a borehole, the remaining samples were packed in sheets wetted with the ÄSPÖ-specific solution and stored in an exsiccator at 100 % air humidity. The resistivity of each samples was measured at different times.

The resistivity of the samples were determined by using the two-point method, where the current  $I$  was injected at the end surfaces of the samples and the voltage drop  $U$  was also measured at the end surfaces. In this case the distance of the voltage electrodes  $a$  in equation 18 will be replaced by the sample length  $L$ .

### 5.4.3 Results

#### ***Samples with different water cement-ratios***

Mixtures with a water-cement ratio of 1:2 and 1:1.133 were not capable of being cast and would have to be stamped. The sample with the higher water-cement ratio of 2:1, however, could be cast.

After setting of about one week the resistivities of the samples were measured. The initial resistivities of the granite-cement mixtures were 4073  $\Omega\text{m}$  (W-C ratio = 1:2), 575  $\Omega\text{m}$  (W-C ratio = 1:1.133), and 304  $\Omega\text{m}$  (W-C ratio = 2:1). After drying at ambient conditions of about two weeks the resistivities increased up to 22514  $\Omega\text{m}$ , 4395  $\Omega\text{m}$ , and 25834  $\Omega\text{m}$ .

The resistivities of the sand-cement mixtures were higher than the granite-cement mixtures. In the initial state the resistivities were 5963  $\Omega\text{m}$  and 8812  $\Omega\text{m}$  (W-C ratio = 1:1.133) and 1730  $\Omega\text{m}$  (W-C ratio = 2:1). For the mixture with the water-cement ratio of 1:1.133 the resistivities increased strongly up to 128022  $\Omega\text{m}$  and 176262  $\Omega\text{m}$  after about two weeks. The resistivity of the water-cement ratio of 2:1 with 74906  $\Omega\text{m}$  was three times higher than the resistivity of the granite-sand mixture.

#### ***Samples produced with an ÄSPÖ specific solution and stored at different conditions***

Both, the granite-cement and sand-cement mixtures produced with a constant ÄSPÖ solution-cement ratio of 1:0.67 were capable of being cast. After setting of about two weeks, the initial resistivities were determined. The mean of the resistivities was 85.3  $\Omega\text{m}$  for the granite-cement mixture and 9186.3  $\Omega\text{m}$  for the sand-cement mixture.

Two granite-cement and two sand-cement samples were stored and dried at ambient conditions. Additionally two other of each were packed in sheets wetted with the ÄSPÖ-specific solution and stored in an exsiccator at 100 % humidity of air.

After about two weeks, the resistivity of the dried sand-cement samples increased up to 83982  $\Omega\text{m}$ . In the same time, the resistivity of the granite-cement mixture resulted to 6222  $\Omega\text{m}$ . Four weeks later, the increase of the resistivities was only slightly higher.

Assuming a saturated rock mass around the geoelectric boreholes, the samples investigated at wet conditions are relevant for the selection of the cementation material.

Due to the adsorption of the ÄSPÖ-specific solution the investigations on the samples stored at wet conditions showed that the resistivities decreased with time of storage for both types of mixtures. The resistivities of the sand-cement mixture (125  $\Omega\text{m}$ ) were approx. 7.8 times higher than the granite-cement mixture (16  $\Omega\text{m}$ ). Table 5-6 shows the results of the samples stored at wet conditions.

The significant high difference of the resistivities could possibly be explained by the granular form of the sand and the crushed granite. Due to the edged granular form of the granite, the pore volume might be higher than in the sand-cement mixture. In the samples with higher pore volume more solution can be stored. The resistivity depends from the saturation and increase with increasing solution content.

The measurements have shown that the resistivities of the sand-cement samples are always higher than of those containing granite powder. The lowest resistivities were determined for the samples produced with an ÄSPÖ-specific solution.

For the cementation of the rock boreholes the sand-cement mixture with a sand-cement ratio of 4:1 produced with ÄSPÖ-solution (ÄS-C ratio = 1:0.67) was selected because the resistivity of the wet cementation material is more similar to the resistivity of the fully saturated granite rock surrounding the measurement boreholes.

The measurements have shown that the resistivities of the sand-cement samples are always higher than of those containing granite powder. The lowest resistivities were determined for the samples produced with an Äspö-specific solution.

For the cementation of the rock boreholes the sand-cement mixture with a sand-cement ratio of 4:1 produced with ÄSPÖ-solution (ÄS-C ratio = 1:0.67) was selected because the resistivity of the wet cementation material is more similar to the resistivity of the fully saturated granite rock surrounding the measurement boreholes.

**Table 5-6** Summary of the results of granite-cement and sand-cement mixtures produced with an ÄSPÖ-specific solution stored at wet conditions

sample	date of measurement	mass m [g]	resistivity $\rho$ [ $\Omega\text{m}$ ]	date of production
sand/cement-ratio = 4:1, ÄS/cement-ratio = 1:0.67				
S-C-ÄS-I	07.12.2001	443.79	13427.2	23.11.2001
S-C-ÄS-I	12.12.2001	451.28	225.7	23.11.2001
S-C-ÄS-I	17.12.2001	455.90	193.9	23.11.2001
S-C-ÄS-I	19.12.2001	459.95	110.0	23.11.2001
S-C-ÄS-I	08.01.2002	461.77	191.8	23.11.2001
S-C-ÄS-I	14.01.2002	466.49	92.9	23.11.2001
S-C-ÄS-II	07.12.2001	421.48	4703.8	23.11.2001
S-C-ÄS-II	12.12.2001	429.36	284.4	23.11.2001
S-C-ÄS-II	17.12.2001	435.06	186.3	23.11.2001
S-C-ÄS-II	19.12.2001	436.96	165.8	23.11.2001
S-C-ÄS-II	08.01.2002	438.67	225.1	23.11.2001
S-C-ÄS-II	14.01.2002	440.90	157.1	23.11.2001
granite/cement-ratio = 4:1, ÄS/cement-ratio = 1:0.67				
G-C-ÄS-1	07.12.2001	401.42	88.8	23.11.2001
G-C-ÄS-1	12.12.2001	414.71	20.8	23.11.2001
G-C-ÄS-1	17.12.2001	421.87	19.2	23.11.2001
G-C-ÄS-1	19.12.2001	426.35	18.3	23.11.2001
G-C-ÄS-1	08.01.2002	438.20	28.6	23.11.2001
G-C-ÄS-1	14.01.2002	444.56	20.9	23.11.2001
G-C-ÄS-2	07.12.2001	403.57	92.2	23.11.2001
G-C-ÄS-2	12.12.2001	420.13	13.1	23.11.2001
G-C-ÄS-2	17.12.2001	428.44	12.3	23.11.2001
G-C-ÄS-2	19.12.2001	434.32	10.9	23.11.2001
G-C-ÄS-2	08.01.2002	451.71	13.8	23.11.2001
G-C-ÄS-2	14.01.2002	459.10	11.3	23.11.2001

### 5.5 Change of Composition of Äspö-Solution by Interaction with Compacted MX-80

These experimental investigations intend to give information about the change of composition which Äspö solution might undergo on its way through compacted MX-80. For the situation given in a deposition borehole filled with blocks of compacted

bentonite it seemed possible that infiltrating solution changes composition not only due to cation exchange processes. It is the micro structure of the built-in material which induces additional effects. Ultrafiltration of solution (the separation of dissolved salts and water) must not be excluded a priori. The phenomenon of ultrafiltration with compacted clays has been described and investigated extensively elsewhere, e. g., (Hanshaw et al. 1973), (Kharaka et al. 1973), (Kharaka et al. 1976), (Demir (a) 1988), (Demir (b) 1988), (Dresner et al. 1963), (Kemper et al. 1964), (Marshall 1948), (Kemper et al. 1963), (Benzel et al. 1984), (Ishiguro et al. 1996). Within the context of this report it is important to note that compaction density, sample height, particle size (or even size of pellets), and method of compaction may have an impact on the course of percolate composition during an experiment. Further, the rate of flow has an impact on the efficiency of ultrafiltration.

For the reasons given, data gained by batch experiments with suspended clay don't give reliable information on the change of solution during infiltration. As the electrical conductivity of aqueous solution depends on mass and composition of its solutes, the change in electrical conductivity for the system compacted bentonite/salt/water may change while the actual water content remains the same. To quantify the possible impact of change in solution composition on the electrical conductivity of partially saturated bentonite it is necessary to know the change of solute composition as Äspö solution protrudes into the clay barrier.

### **5.5.1 Materials and Methods**

The experiment being conducted is done with a cell normally taken for the determination of swelling pressures. The bottom frit of the pressure cell was covered with filter paper to prevent it from clogging. 16.1 g MX-80 representatively probed were placed on it and treated with a spatula to produce an approximately horizontal surface. Compaction proceeded with ca. 1 MPa/min (with sample radius of 2.5 cm, this gives 1901 N/min) to a sample height of 0.51 cm giving a dry density of 1.66.

Compaction pressure was held constant for 15 min to ensure de-airation of the sample. Then the sample was allowed to relax by deloading it. After 1 min, the sample was compacted again to the desired height and the load held constant for again 15 min. This procedure was repeated until no relaxation occurred anymore and thereby a

sample was obtained consolidated at a dry density of  $1.66 \text{ g/cm}^3$ . The uncertainty of dry density was  $\pm 0.01 \text{ g/cm}^3$ .

The piston was fixed with the screw cap on top. This way, the exact geometry of the sample is known throughout the experiment.

The general set up of the experiment is shown in Figure 5-12.

The gas-filled headspace of containments for both inflowing and outflowing solution were connected via capillary tubes with small bottles of Äspö solution to prevent evaporation during the experiment. Containments for outflowing solution were changed at intervals ranging between 1 and 4 days. By appropriate weighing an exact mass balance was maintained for inflowing and outflowing solution, and hence for the percolated bentonite.

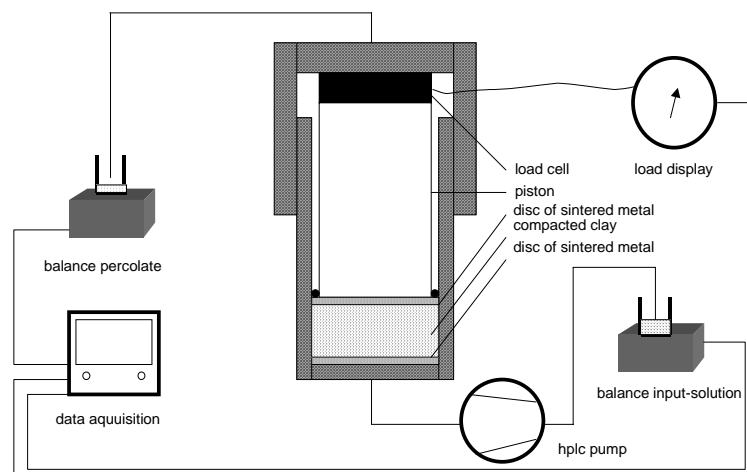


**Figure 5-12** Experimental set-up of percolation experiment

The HPLC-pump delivers the solution at a constant rate of  $0.0020 \pm 0.0003 \text{ ml/min}$  up to a maximum fluid pressure of 47 bar. This corresponds to the maximum likely hydrostatic pressure in the Äspö URL. Also the pump rate compares well with the maximum seepage rate given by SKB. The experiment is run under ambient temperature conditions, which by daily measurement is given with  $22.1 \pm 0.7 \text{ }^\circ\text{C}$ .

The discontinuously taken percolates are characterized by the measurement of their density and concentrations of Na, K, Mg, Ca, and SO<sub>4</sub>. Concentration of chloride is calculated by difference.

The composition of inflowing "Äspö solution" was calculated as the mean of 55 single sets of analytical data as delivered by SKB. Minor solute components were neglected. With a small correction for electroneutrality, the composition given in Table 5-1 was obtained. Figure 5-13 gives an overview of the variation of probed Äspö solution with sampling date. Table 5-7 summarizes details of the experiment.

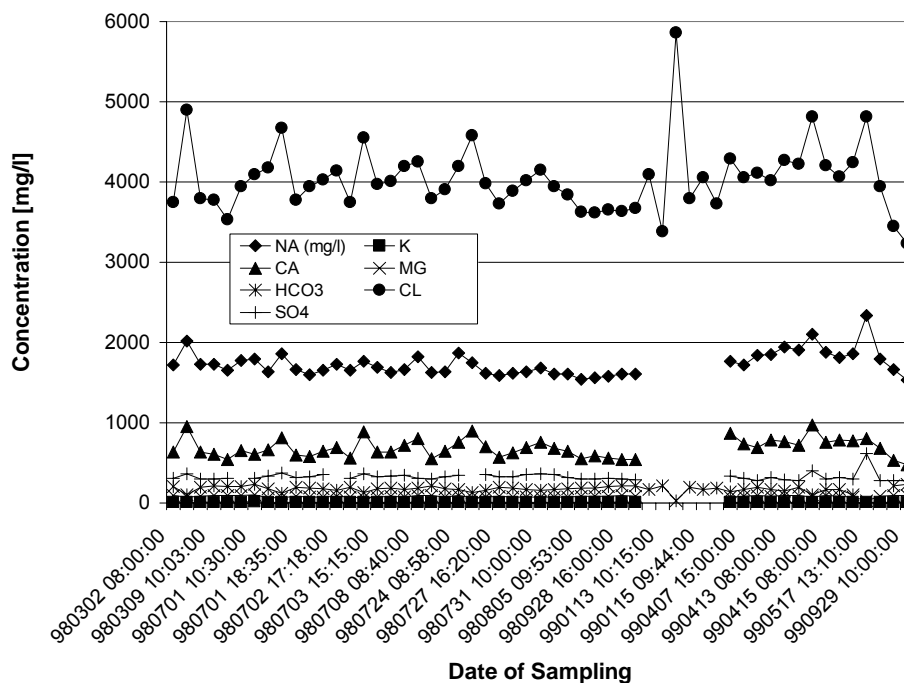


**Figure 5-13** Composition of Äspö solution. All concentrations in mg/l.

### 5.5.2 Results

Criteria for the termination of the experiment were initially planned to be constant values for outflowing solution density and composition (which should be the same like the one of inflowing Äspö solution). However, when the experiment was terminated, a condition of equilibrium between Äspö solution and sample had not been established yet.

**Table 5-7** Planning data for percolation experiment

Diameter of sample:	r =	2.46	[cm]
	h =	0.51	[cm]
Volume of sample:	V =	9.7	[cm <sup>3</sup> ]
Grain density of MX-80:	$\rho_G$ =	2.439	[g/cm <sup>3</sup> ]
Target density:	$\rho_{\text{Target}}$ =	1.66	[g/cm <sup>3</sup> ]
Necessary mass of MX-80:	$m_{\text{Clay}}$ =	16.1	[g]
CEC:	CEC =	0.73	[mol <sub>c</sub> /kg]
CEC of sample:	$\text{CEC}_{\text{Sample}}$ =	0.01175	[mol <sub>c</sub> ]
Grain volume of sample:	$V_G$ =	6.6	[cm <sup>3</sup> ]
Remaining pore volume:	$V_P$ =	3.1	[cm <sup>3</sup> ]
Normality of Äspö solution:	$N_{\text{Solution}}$ =	120.58	[mmol/l]
Charges in 1 pore volume Äspö solution:	$q_{VP}$ =	0.00037	[mol <sub>c</sub> ]
Necessary pore volumens for 1 x $\text{CEC}_{\text{Sample}}$ :	$n_{VP}$ =	31.5	[1]
corresponding to	$V_{\text{CEC}}$ =	97.4	[cm <sup>3</sup> ]
Powder density of MX-80:	$\rho_{\text{bed}}$ =	1.034	[g/cm <sup>3</sup> ]
Bed depth:	$h_{\text{bed}}$ =	0.82	[cm]
Target rate of flow:	$J_{\text{normed}}$ =	1	[cm <sup>3</sup> /cm <sup>2</sup> *d]
Cross sectional area of sample:	A =	19.0	[cm <sup>2</sup> ]
Total rate of flow:	J =	19.0	[cm <sup>3</sup> /d]
corresponding to	J =	0.79	[cm <sup>3</sup> /h]
corresponding to	J =	0.013	[cm <sup>3</sup> /min]

The change in solution composition is depicted in Figure 5-14 to Figure 5-20. All measured concentrations were related to the total mass of percolated solution. This is not exactly, but quite the mass of water percolated. The first data point in all cases represents the inflowing Äspö solution. Its value is marked by a horizontal “baseline” in each figure. In general, it may be concluded that at the beginning of the experiment the sample takes up Mg and Ca from solution while Na and K are being released. The second data point (which represents the first solution having left the sample) indicates dissolution of some minor components of MX-80. As the normality of percolate remains to be higher than that of Äspö-solution, this process seemingly remains to continue during the whole experiment. It cannot be explained with cation exchange. This becomes obvious when the normality of the percolate is regarded (Figure 5-14).

It is defined as

$$N = c_{\text{Na}} + c_{\text{K}} + 2 \cdot (c_{\text{Mg}} + c_{\text{Ca}}) \quad (21)$$

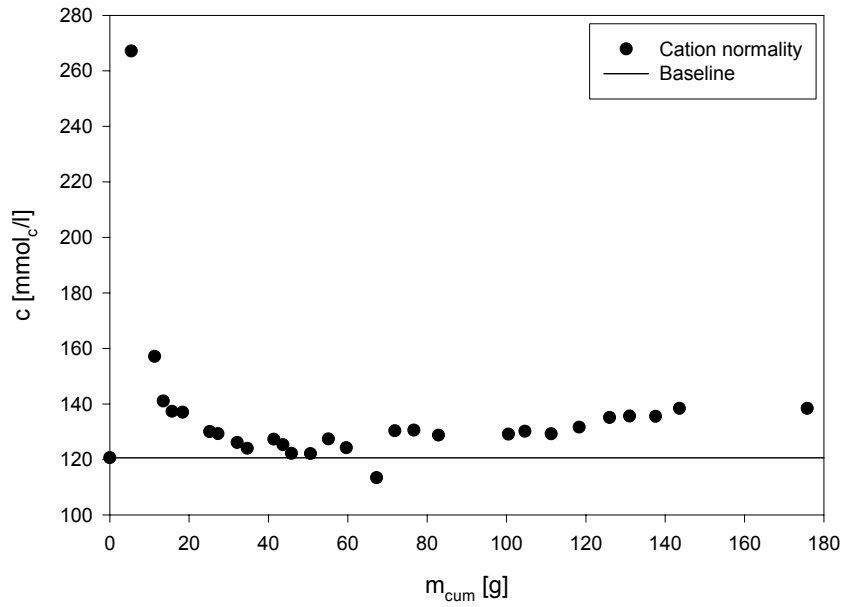


**Figure 5-14** Change of normality of percolate. Note that normality is constantly a bit higher than that of inflowing solution

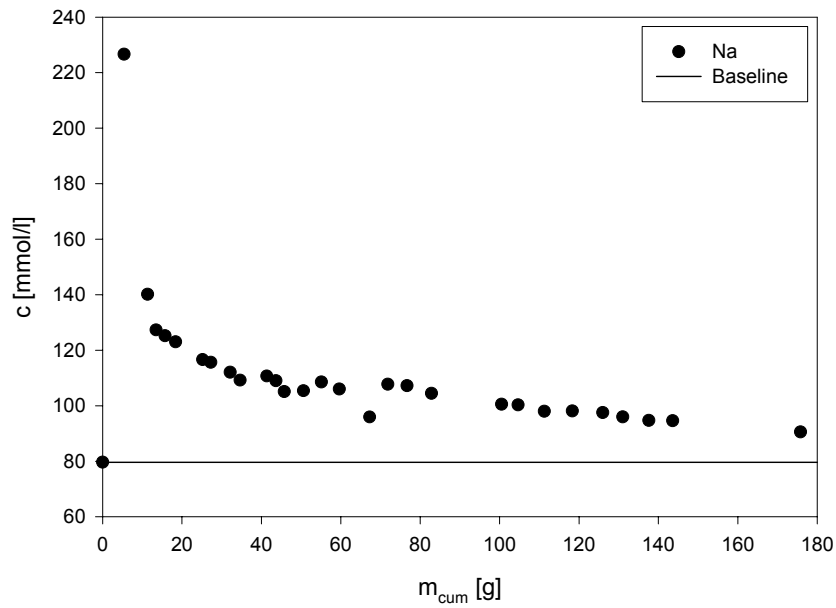


**Figure 5-15** Na-concentration in Äspö-solution after penetrating compacted MX-80

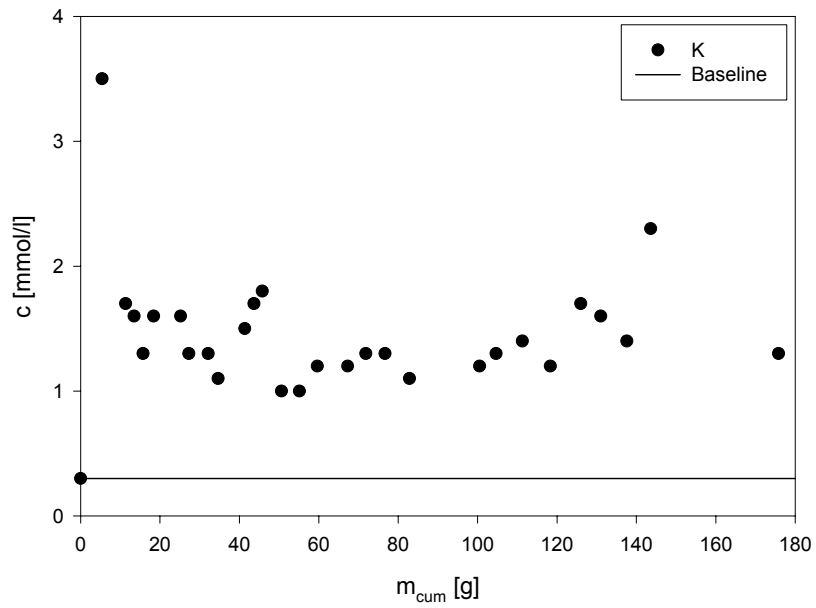


**Figure 5-16** K-concentration in Äspö-solution after penetrating compacted MX-80

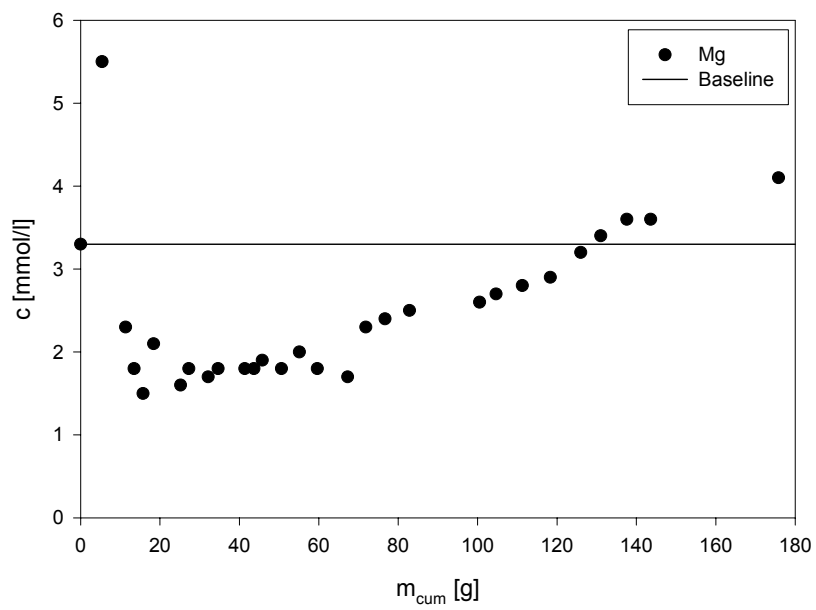


**Figure 5-17** Mg-concentration in Äspö-solution after penetrating compacted MX-80

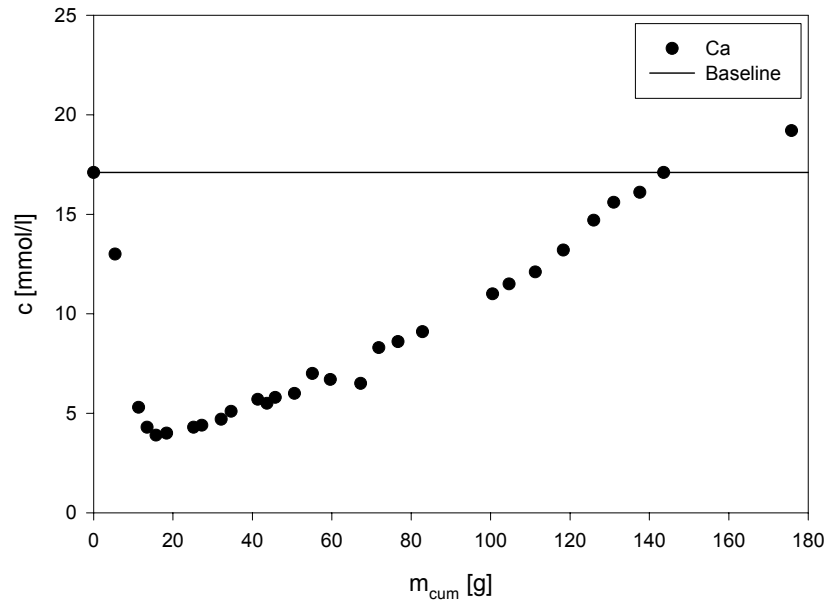


**Figure 5-18** Ca-concentration in Äspö-solution after penetrating compacted MX-80

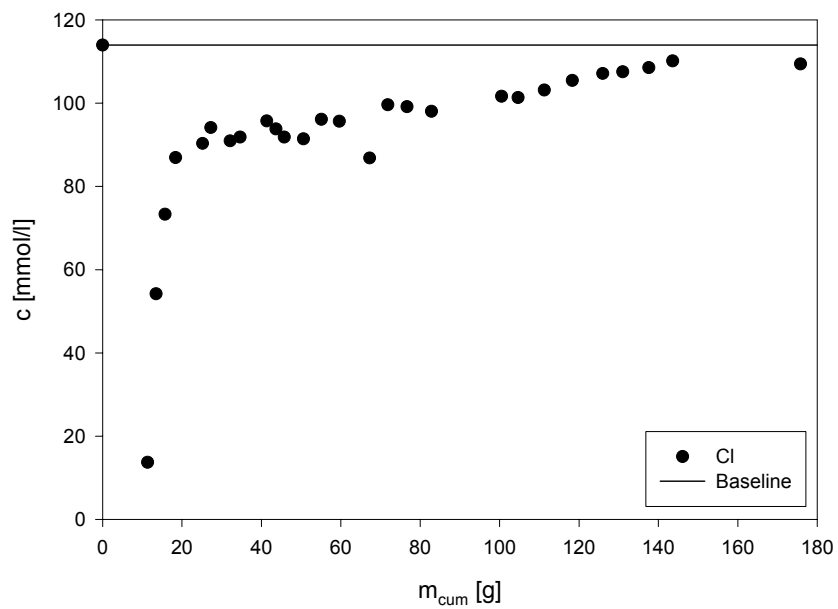


**Figure 5-19** Cl-concentration in Äspö-solution after penetrating compacted MX-80

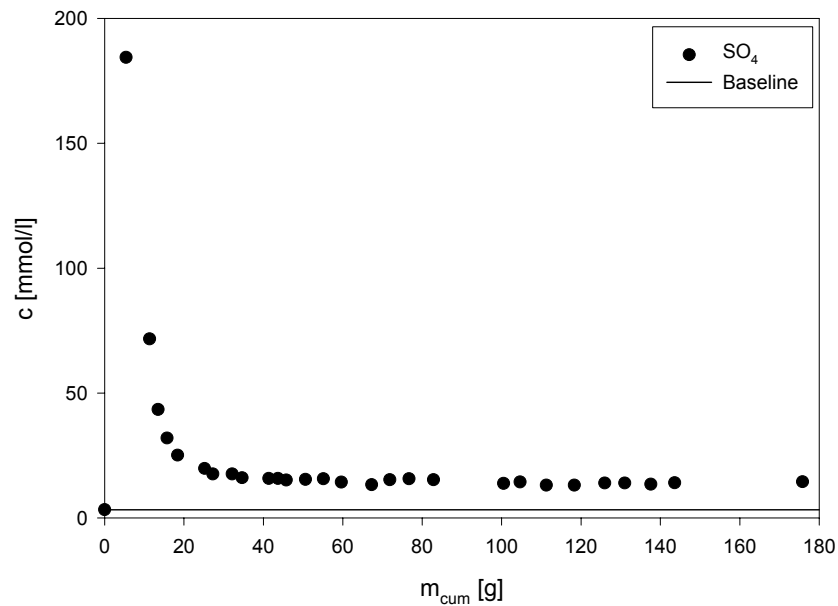


**Figure 5-20** SO<sub>4</sub>-concentration in Äspö-solution after penetrating compacted MX-80

With the first solution entering the clay, salt is mobilized which adds to the total salinity introduced by the Äspö solution. On the grounds of purely cation exchange reasoning, also the increase in sulfate would not be expected. This might be due to the oxidation of pyrite present in the material. The content of chloride was calculated from the charge difference of the cations (Na, K, Mg, Ca) and sulfate.

Figure 5-19 shows that the content of chloride in the very first volume increments is replaced in favour of sulfate. At the end of the experiment, chloride concentration is still lower than that of the inflowing solution, while in the contrary, sulphate continues to be mobilized from the sample.

From the salt content in the percolate, the compacted MX-80 under the given conditions of salinity, flow rate, and compaction density does not seem to behave like a semipermeable membrane. After an initial increase in salinity, the overall salt content in terms of normality comes very close to but is not exactly like the one of the inflowing solution.

Generally, three processes can possibly occur within the sample: cation exchange, mineral dissolution, and ultrafiltration.

**Cation exchange.** At low ionic strengths this reaction proceeds charge-neutrally. That means that for any charge transferred into the adsorber phase a same charge is *exchanged* into the solution phase. Due to the formation of chloro complexes with alkaline earth metals, this law seemingly is not fulfilled. What is the extent of chloro complex building in Äspö-solution? Taken the stability constant for  $\text{CaCl}^+$  at 298.15 K and 1 atm pressure (Johnson 1979) (Johnson 1981):

$$\log K_{\text{CaCl}^+} = 0,42 \quad (22)$$

This is in a certain proportion to the conditional stability constant (Sposito 1989):

$$\log K_{\text{CaCl}^+} = \log^c K_{\text{CaCl}^+} + 0,512 \left[ \frac{\sqrt{I}}{1 + \sqrt{I}} - 0,3I \right] \Delta Z^2 \quad (23)$$

with

$$\Delta Z^2 \equiv \nu_c m^2 + \gamma + \nu_a I^2 - (\nu_c m + \gamma - \nu_a I)^2 \quad (24)$$

In the preceding equation, the valences of any constituent building up the complex with the general formula  $\text{M}_{\nu_c}^{m+} \text{H}_{\nu_a}^{+} \text{L}_{\nu_a}^{-}$  are accounted for. With the ionic strength pertinent for Äspö-solution, equations 22 and 23 give after rearrangement:

$$\frac{[\text{CaCl}^+]}{[\text{Ca}^{2+}]} = 10^{0,18} [\text{Cl}^-] \quad (25)$$

Equation 25 may be solved iteratively to give a set of mutually consistent sets of constituent-concentrations,  $\log K_{\text{CaCl}^+}$  and ionic strength. For the present purpose it might be sufficient to make an estimate by introducing the pertinent chloride concentration in Äspö-solution. The result is that about 14.5 % of total dissolved calcium (and presumeably Mg) is present as monovalent chloro complex, giving rise to (seemingly) non-electroneutral cation exchange. Practically, this means for the present case that by the adsorption of Ca and Mg (as  $\text{CaCl}^+$  and  $\text{MgCl}^+$ , respectively) cation normality in solution decreases.

The observed change of composition of percolate indicates that Mg and Ca are adsorbed in favour of Na and K. It is hypothesized that both cations are at least partially adsorbed in the form of their chloro complexes. This is in accordance with the

systematically "too low" concentration of chloride as compared with its input concentration. On the other hand, chloride is not likely to be removed from solution by precipitation, because geochemical calculation does not indicate saturation of any chloride-bearing mineral phase (see below).

In the last increments of percolate, however, Mg and Ca begin to be released from the sample. Thus, the overall trend of cation concentrations seems to indicate that the dominating process at the end of experiment is mineral dissolution rather than cation exchange.

**Mineral dissolution.** MX-80 bentonite contains a number of accessory minerals, e. g., calcite and pyrite. These minerals are likely to dissolve upon contact with Äspö-solution. Mineral dissolution will tend to enhance salinity of solution, i. e., cation and anion normality.

The observed change of composition with respect to sulfate indicates that mineral dissolution happens to some degree, because sulfate is not involved in cation exchange. Geochemical modelling (EQ36) indicates no saturation whatsoever (Figure 5-21). However, this information must be regarded with caution, because due to the small volumes of percolate taken at each increment, no carbonate contents could be determined. As MX-80 contains appreciable amounts of calcite it might well be possible that the percolate contains small amounts of carbonate adding to the charge balance constraint which served as base of calculation for chloride content.

**Ultrafiltration.** As mentioned above, compacted clays may behave like semipermeable membranes, retaining salt and rendering the percolating solution to a lower salinity. This effect would have a considerable impact on the electrical conductivity of the solution. However, the obtained data do not indicate any ultrafiltration to occur under the conditions applied.

Letting aside ultrafiltration, cation exchange and mineral dissolution will occur simultaneously within the sample. Ultimately, percolating solution should exhibit the

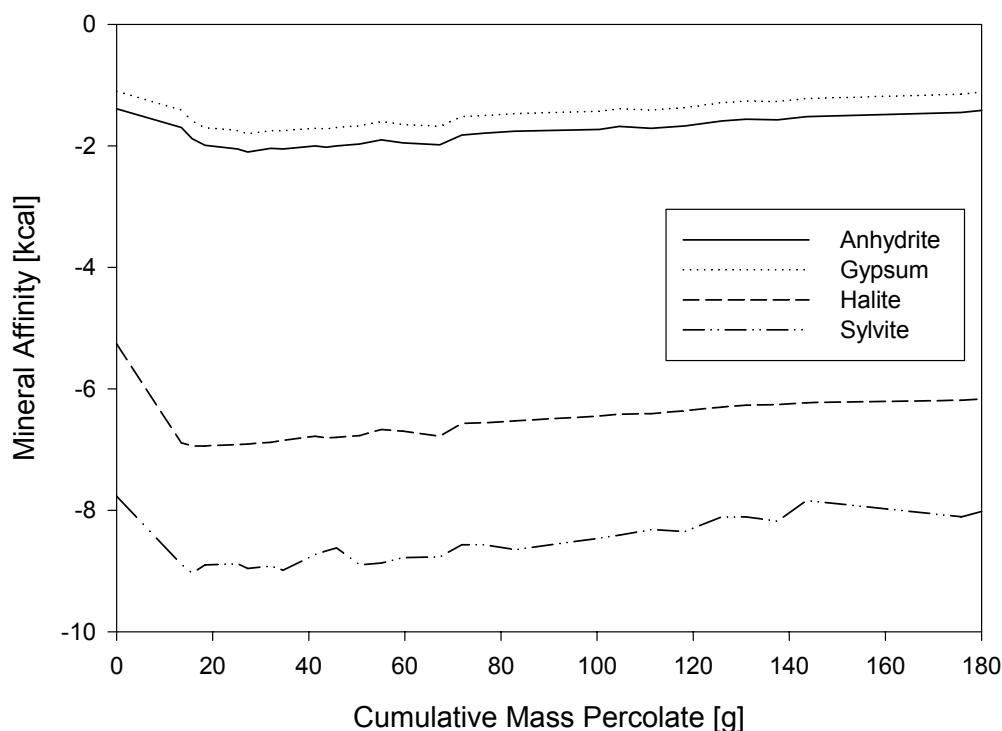


**Figure 5-21** Mineral saturation states in percolates

same composition like the inflowing solution. Since this is not the case, either of both processes has not come to an end. We consider mineral dissolution as being the rate controlling process with cation exchange equilibrium establishing itself accordingly. The almost linear course of sulfate indicates a state of stationary equilibrium where some accessory mineral (perhaps pyrite) dissolves.

Approximately 30 pore volumes have penetrated the sample which is about one surface charge in terms of dissolved cations. The mass of penetrated solution exceeds the six-fold of the mass of bentonite.

This experiment was initiated by the “fear” that compacted bentonite could act as semipermeable membrane. By the retention of salt, electrical conductivity would have been significantly diminished. The results show that under the given conditions of solution composition, flow velocity, compaction density, layer thickness, temperature and bentonite composition no salt retention is observed. The overall salinity of solution, however, is higher than that of Äspö-solution, which we suppose to be the consequence of mineral dissolution. Whether this leads to a changing electrical conductivity of solution depends on the partial molar conductivity of each species present and needs to be measured in artificial solutions.

## 6 Assessment of Measurement Resolution

On the basis of the laboratory calibration results, model calculations were performed in order to assess the measurement resolution which could be expected from the in-situ measurements and to support the design of the electrode arrays.

According to the laboratory calibrations, the buffer and backfill material should already have a rather small resistivity around 7  $\Omega\text{m}$  and 16  $\Omega\text{m}$ , respectively, when installed (at a water content of 12 to 13 wt.%). In conjunction with the comparably high resistivity of the rock (above 1000  $\Omega\text{m}$  at full saturation), this could have the effect that resistivity reductions by increasing water uptake in the buffer and backfill could not be properly detected if all electrodes for the buffer measurements were located in the rock or the electrodes in the backfill were located too close to rock. In order to clear this issue, model calculations were performed to determine optimum electrode arrangements, enabling high resistivity resolution.

Modelling was performed by calculating the expected measurement values for a given set of measurement configurations. Afterwards, the artificial measurement values were evaluated by inverse modelling (compare chapter 3.2).

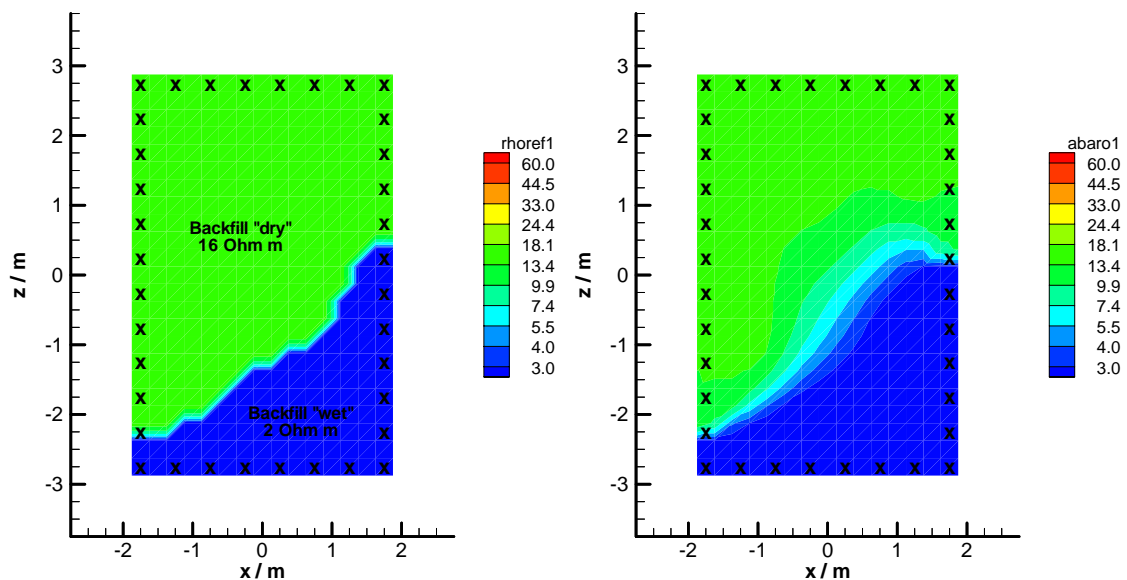
### 6.1 Backfill

Results of geoelectric modelling of the prototype repository drift using an elliptic drift model were not satisfying with an electrode configuration around the drift surface, which was the first approach. The presence of the surrounding high-resistive rock seemed to cause a high-resistivity “ghost” anomaly in the drift center. In order to clear up whether this result was due to insufficiencies of the employed computer code or whether it is inherent to the model and electrode configuration, two simplified rectangular models were investigated.

In both models, the drift has a rectangular cross section, and the electrodes (36 in total) are located along the drift surface. In the first model, there is no surrounding rock, that means the backfilled drift is isolated. In the second model, a highly resistive rock (1000  $\Omega\text{m}$ ) surrounds the drift. The drift itself consists of a lower “wet” backfilled part (2  $\Omega\text{m}$ ) and an upper “dry” backfilled part (16  $\Omega\text{m}$ ). Modelling was performed by

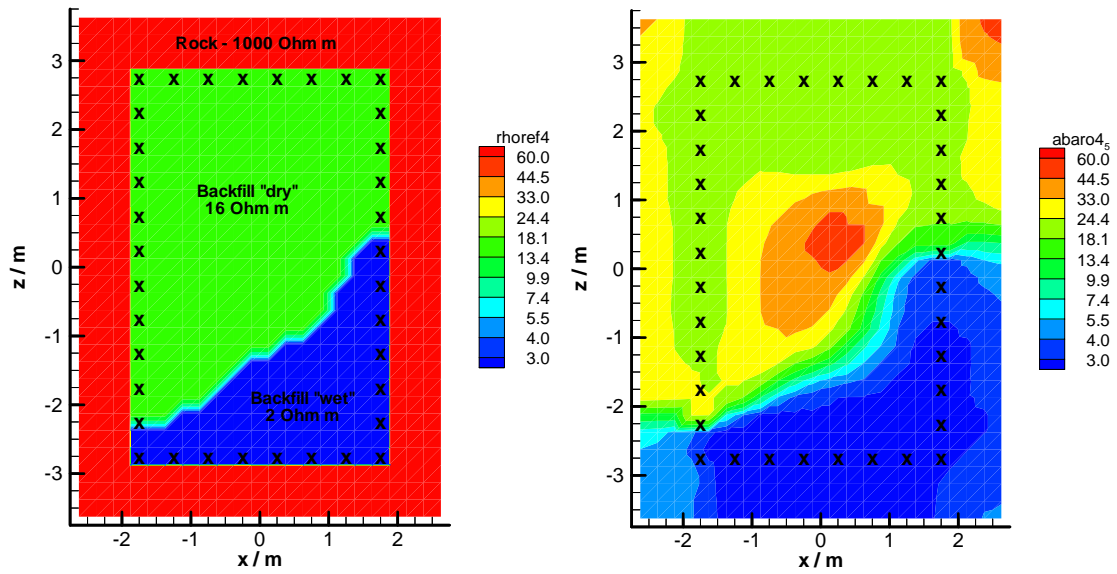
calculating artificial measurement results from the input model and afterwards performing an inversion of the “measured” data.

Figure 6-1 shows the first input model (left) and the corresponding inversion result (right). Obviously, the input model is well reconstructed by the inversion algorithm. The resolution is satisfying.



**Figure 6-1** Geoelectric modelling of the prototype repository backfill: Rectangular model without surrounding rock (left: input model, right: inversion result)

The second input model (with rock) and the corresponding inversion result are shown in Figure 6-2. Here, the high-resistivity ghost in the drift center appears again. That means the ghost does not result from an disadvantageous geometry in the original elliptic drift model, but is created as soon as the highly resistive rock is included in the model. Placing all the electrodes on the border between rock and drift will, in any case, cause this problem. Since the rock is there in reality, it cannot be left out in the model. Therefore, the only solution is an altered electrode configuration. Modelling with the elliptic drift model and different electrode configurations have shown that adequate results can be expected if a double cross electrode array as shown in Figure 6-3 is being installed. The “measured” resistivity change is reconstructed sufficiently in this case.



**Figure 6-2** Geoelectric modelling of the prototype repository backfill: Rectangular model with surrounding rock (left: input model, right: inversion result)

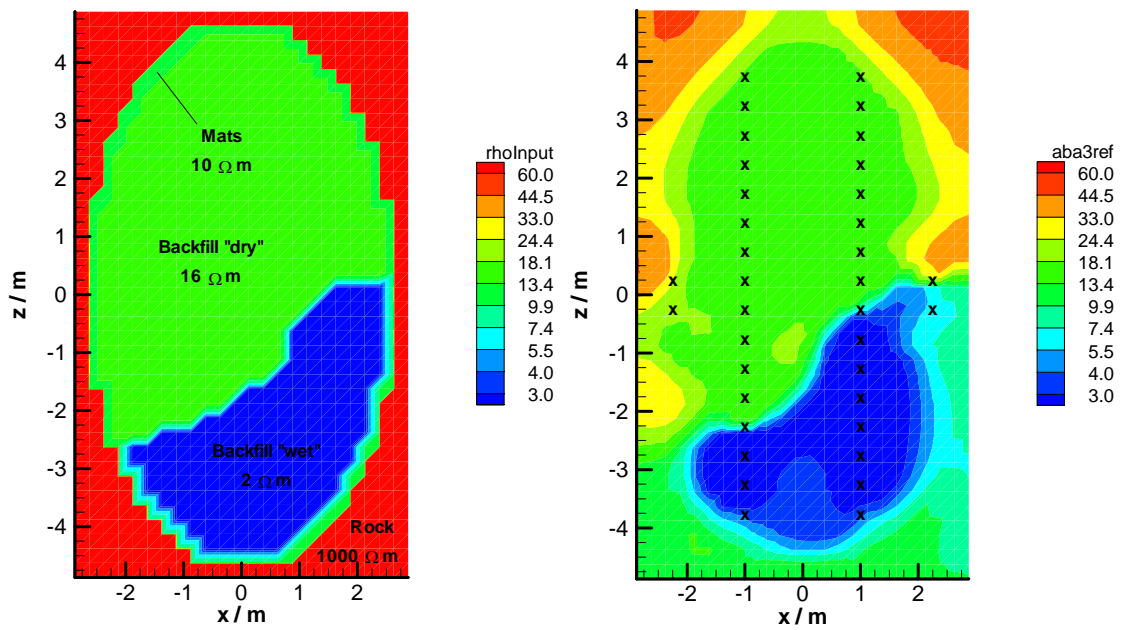


**Figure 6-3** Geoelectric modelling of the prototype repository backfill: Elliptic drift model with surrounding rock (left: input model, right: inversion result); “double cross” electrode arrangement (x = electrode locations)

## 6.2 Buffer

Various models were investigated in order to determine the most adequate electrode arrangement for the buffer. The first model used the originally planned arrangement of four electrode chains located outside the buffer in the rock. This led to completely insufficient results for the buffer. Further modelling included an additional electrode chain centered in the buffer or a chain placed horizontally on the buffer surface. While the horizontal chain gave only little improvement, the additional central chain led to better results when the buffer was modelled as homogeneous dry ( $7 \Omega\text{m}$ ) or homogeneous wet ( $4 \Omega\text{m}$ ). For the most interesting case, however, which incorporates a partially wetted buffer, again no satisfying results could be achieved. The modelling results with the original model, the model with an additional central electrode chain, and with a horizontal chain are shown in Figure 6-4 to Figure 6-6.

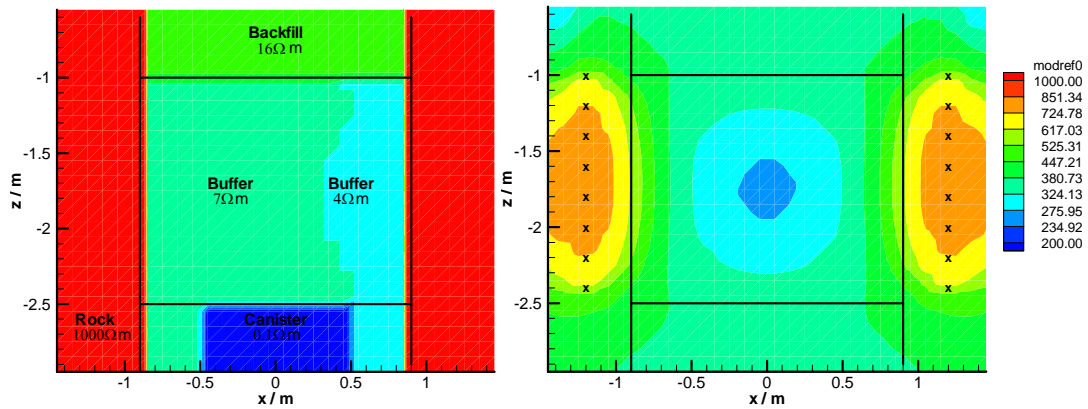


**Figure 6-4** Geoelectric modelling of the prototype repository buffer with the original electrode arrangement (left: input model, right: inversion result)

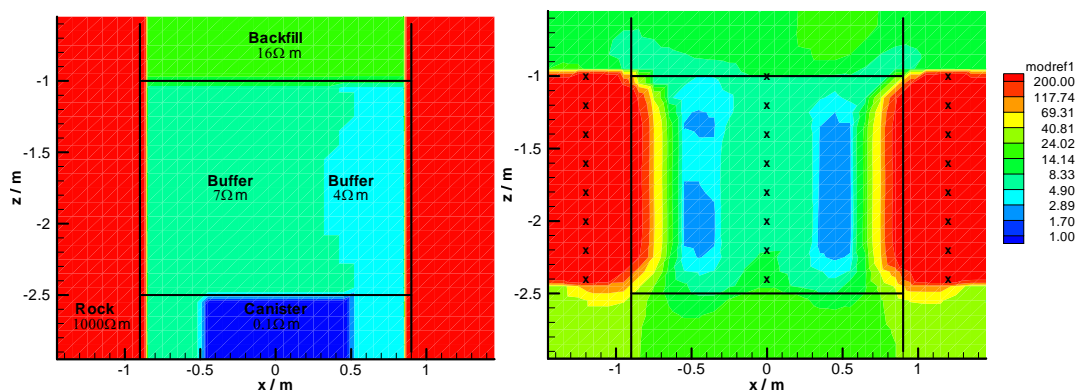


**Figure 6-5** Geoelectric modelling of the prototype repository buffer with additional central chain (left: input model, right: inversion result)

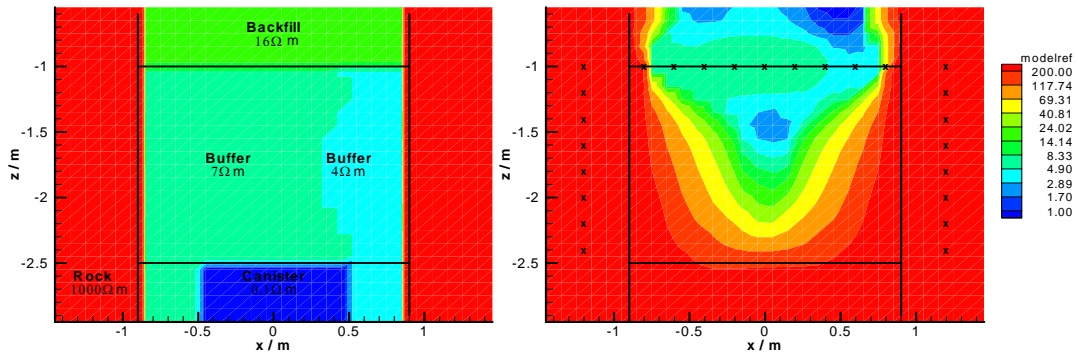


**Figure 6-6** Geoelectric modelling of the prototype repository buffer with additional horizontal chain (left: input model, right: inversion result)

In order to get a better resolution for the buffer resistivity distribution, a new electrode arrangement featuring two vertical chains in the buffer was agreed. One chain should be placed near the centerline of the buffer and the other near the borehole wall. A third electrode chain in the rock at the original location is also kept.

With this electrode arrangement a new modelling series was started. Figure 6-7 to Figure 6-9 show the results for a dry buffer, for a small wetted zone near the wall, and for an enlarged wetted zone.

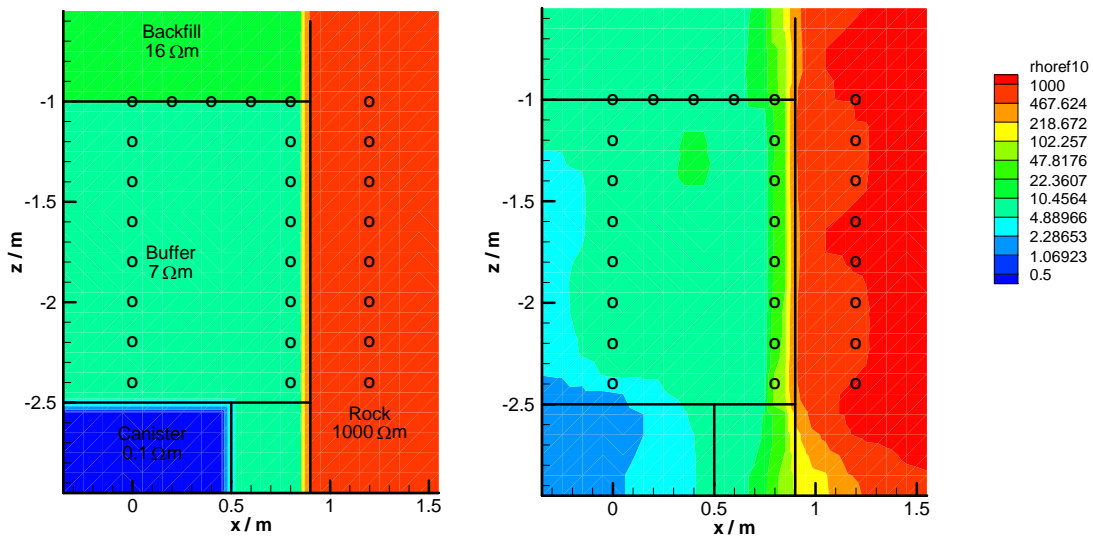


**Figure 6-7** Geoelectric modelling of the prototype repository buffer with the new electrode arrangement: dry buffer (left: input model, right: inversion result)

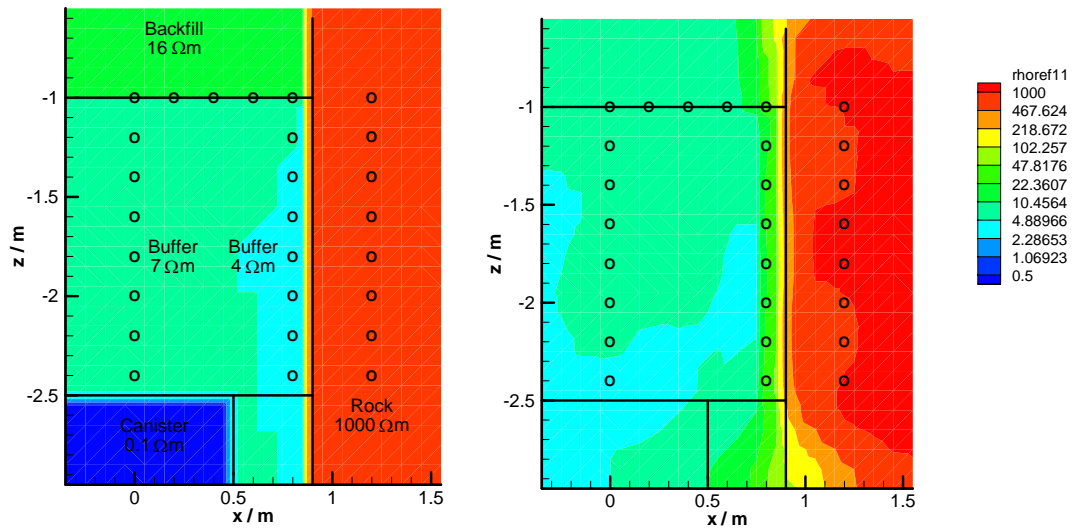


**Figure 6-8** Geoelectric modelling of the prototype repository buffer with the new electrode arrangement: partially wetted buffer (left: input model, right: inversion result)

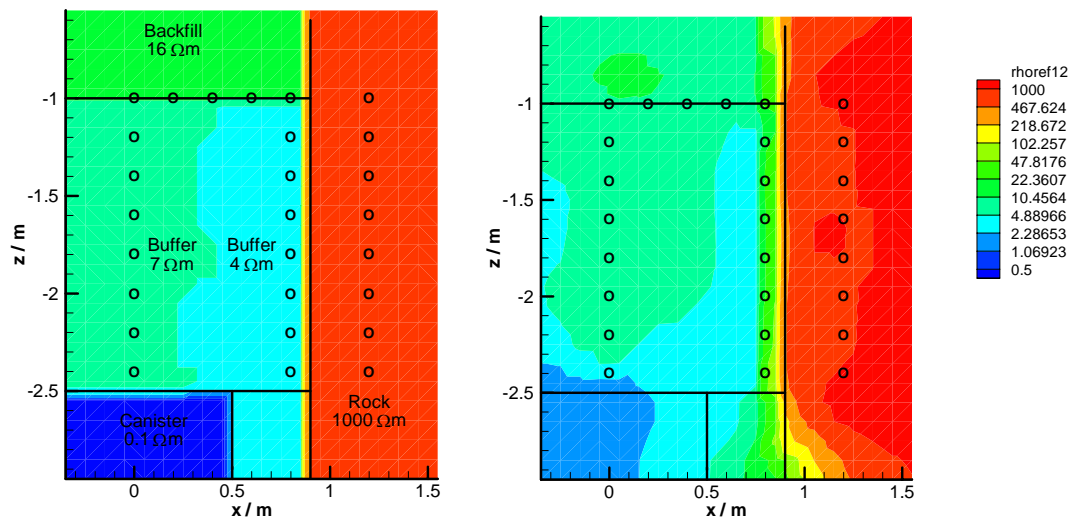


**Figure 6-9** Geoelectric modelling of the prototype repository buffer with the new electrode arrangement: enlarged wet buffer zone (left: input model, right: inversion result)

The figures show that although there are some deviations from the input model, especially at the left model border and near the heater, the buffer resistivity distribution is fitted rather well. The most interesting region near the borehole wall is modelled in a reliable way. In particular, no high or low resistivity “ghosts” are generated, as for instance in Figure 6-5. Therefore, this electrode arrangement appeared adequate for the planned investigation.

## **7 Field Measurements**

### **7.1 Backfill Section I**

The array in the backfill in Section I was the first one to be installed. Measurements started in October 2001. Figure 7-1 shows on the upper left side the resulting resistivity distribution of the first measurement. The initial resistivity of the backfill ranged around 10 to 14  $\Omega\text{m}$ , corresponding to a water content of 13 to 14 %. In the lower part of the backfill the resistivity was somewhat higher, which is due to a lower density of the backfill near the floor (a consequence of the installation and compaction procedure).

Since the first measurement the resistivity of the backfill has been steadily decreasing, starting near the walls of the tunnel and continuing to the center. This is clearly visible in the corresponding tomograms of Figure 7-1. The water uptake from the tunnel walls and the lower saturation in the center is also confirmed by suction measurements performed by Clay Technology (Goudarzi & Börgesson, 2003).

Until February 2004, a very homogeneous resistivity distribution was reached; with a value of 3 to 5  $\Omega\text{m}$  corresponding to a water content around 20 %. According to the calibrations, full saturation ranging around 2  $\Omega\text{m}$  has not yet been achieved. There has, however, also been a slight temperature rise in the tunnel (to maximal 32 °C) which may cause an additional resistivity decrease. This is limited, however, to less than 1  $\Omega\text{m}$  (see Section 5.2.2), which means water content may be lower by 0.5 to maximal 1 %.

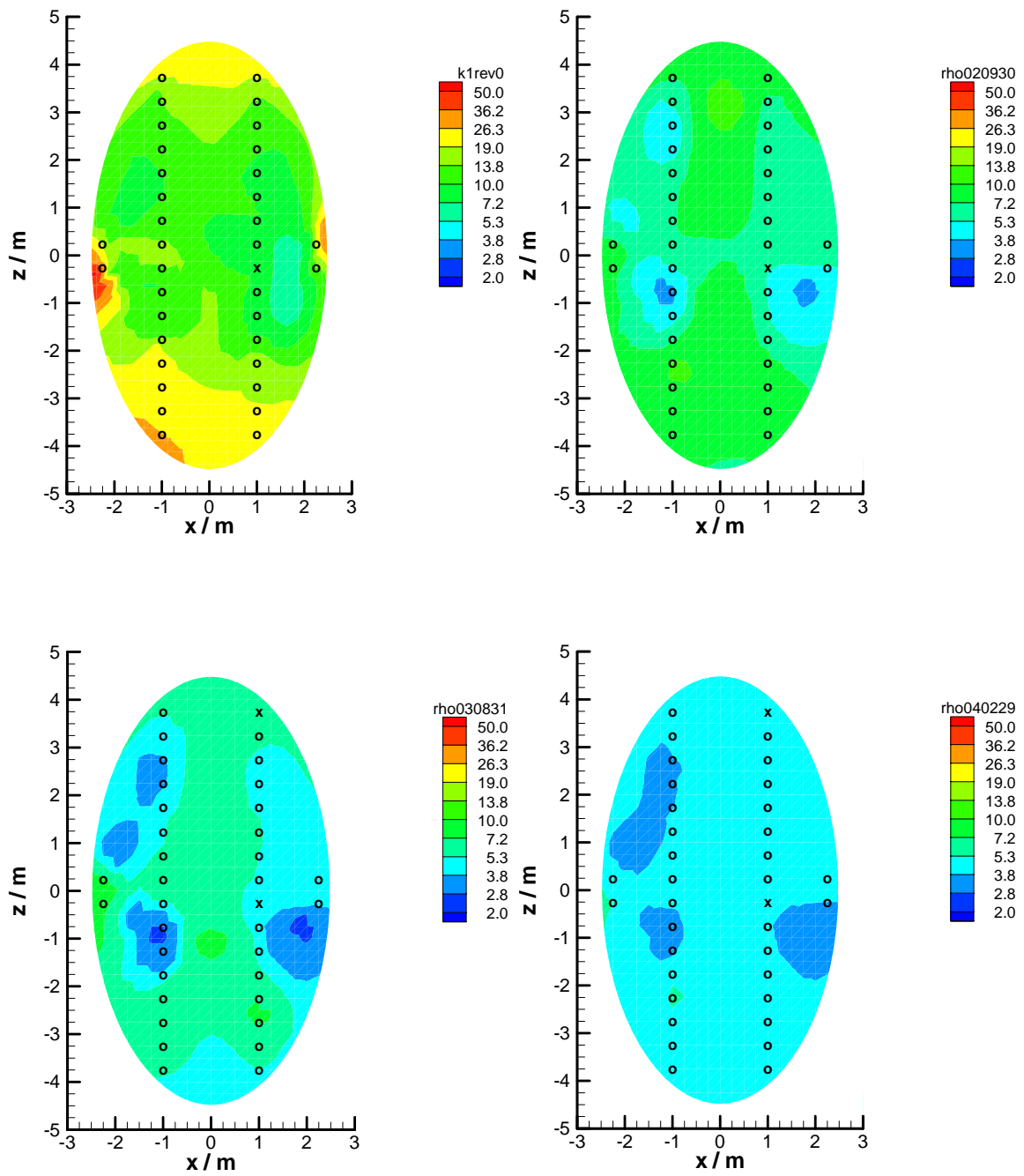


**Figure 7-1** Resistivity distribution in Backfill Section I, October 2001 (upper left), September 2002 (upper right), August 2003 (lower left), and February 2004 (lower right)

## 7.2 Backfill Section II

The array in the backfill in Section II has only been installed in June 2003. The results of the first measurement (Figure 7-2, left side) show a much lower resistivity than the early measurements in Section I. Obviously, the backfill had a considerably higher water content already during installation. This observation was also made during instrumentation when significant amounts of water were found flowing in from the tunnel walls. Consequently, resistivity has been decreasing further from the tunnel walls (Figure 7-2, right side). Close to the walls it ranged around  $3 \Omega\text{m}$  in February 2004; the backfill is therefore not far from full saturation. In the center resistivity was between  $5$  and  $8 \Omega\text{m}$  corresponding to a water content of about 15 to 18 %. The resistivity distribution is much less homogeneous than in the backfill of Section I, with a higher contrast between tunnel periphery and center. This is probably a consequence of higher water inflow rates.

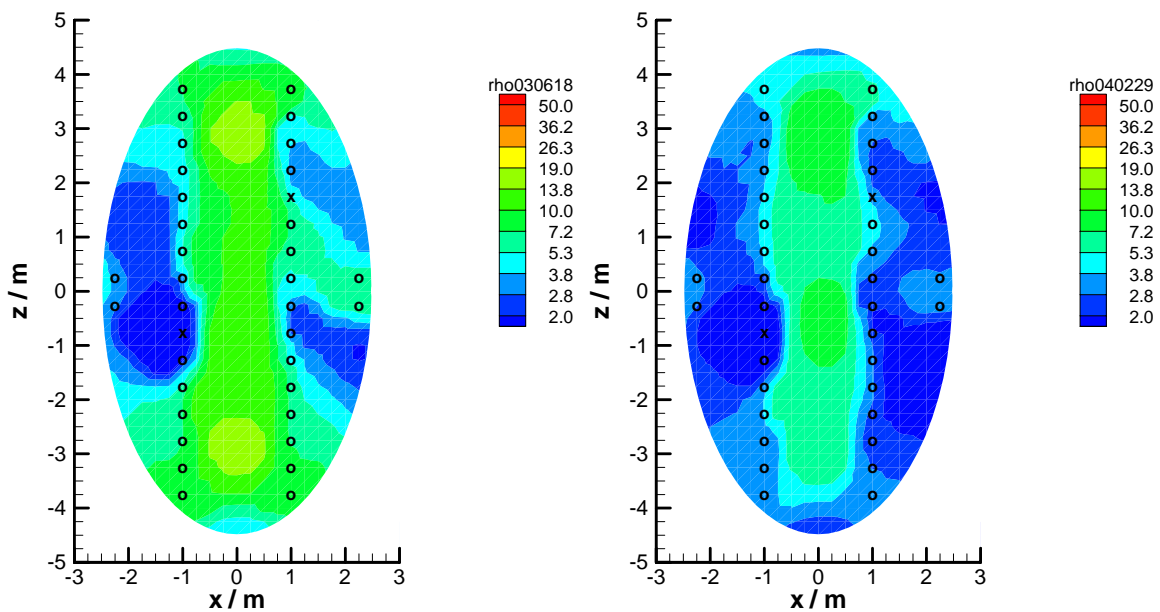


**Figure 7-2** Resistivity distribution in Backfill Section II, June 2003 (left) and February 2004 (right)

### 7.3 Buffer

The results of the first measurement taken in May 2003 (Figure 7-3, left side) show the high resistivity (above 1000  $\Omega\text{m}$ ) of the rock on the right side and the low resistivity of the buffer (below 80  $\Omega\text{m}$ ) on the left. The picture is somewhat distorted by the fact that along the electrode chains the resistivity is increased compared to the undisturbed buffer. The increased resistivity along the electrode chains can be attributed to the refilling of the electrode boreholes with bentonite powder produced during borehole drilling. It was, however, expected that the difference would diminish with time, especially if the buffer was taking up water. Indeed, a progressing decrease of resistivity in the buffer was observed during the following months. In February 2004 (Figure 7-3, right side), the resistivity near the electrode chains was no longer higher than in the surrounding buffer. While the overall behaviour is rather clear, it is difficult to interpret buffer resistivity in terms of water content. Near the electrode chain in the centre of the buffer (left in the tomograms), the resistivity ranged between 4 and 24  $\Omega\text{m}$ . The observation that the lowest resistivities are found near the top center of the buffer gives rise to the presumption that the water enters the buffer from the top, i. e., from the backfilled tunnel. In particular, there is no hint that significant amounts of water are drawn from the rock near the borehole wall into the buffer. This is confirmed by the measurements in the rock boreholes (see next section).

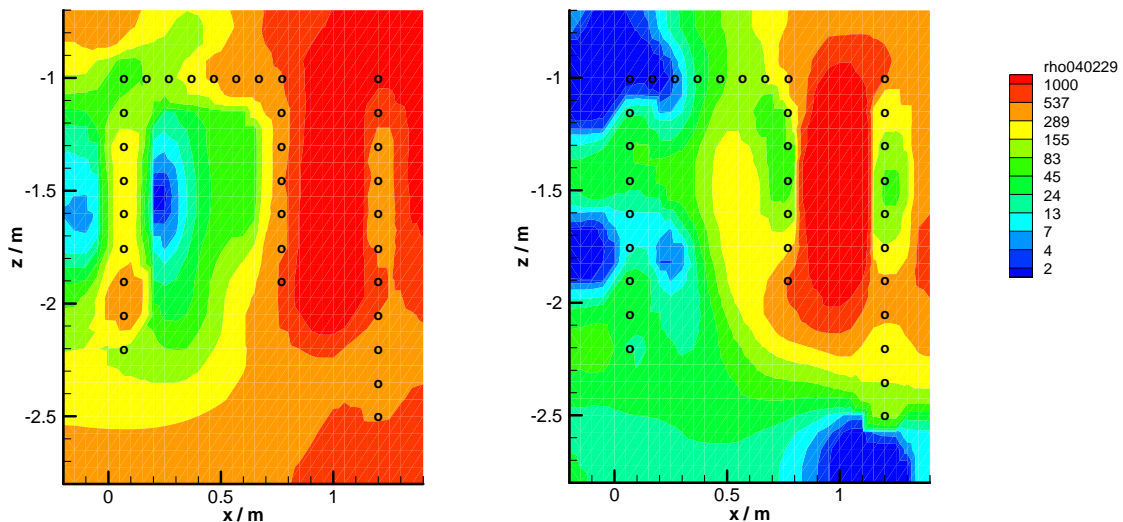


**Figure 7-3** Resistivity distribution in the buffer at the top of deposition hole 5, May 2003 (left) and February 2004 (right)

## 7.4 Rock

The resistivity distributions along the three electrode chains installed in the rock are quite similar to each other and show no significant variation in time until April 2003 (Figure 7-4 through Figure 7-6). Close to the electrodes, the resistivity ranges around 200  $\Omega\text{m}$ . This value characterizes the water-saturated concrete used for backfilling the electrode boreholes. Further away from the boreholes, the resistivity rises to values of 2000 to 7000  $\Omega\text{m}$  which is characteristic for granite. Figure 7-4 (left side) shows the resistivity distribution around the chain KA 3550 G04 in the rock near deposition hole 5. From April 2003 on, there is a slight decrease in resistivity in the rock near deposition hole 5 (Figure 7-4, center and right side). This coincides with installation of the buffer which also stopped the pumping of water from the open deposition hole. Apparently, this had caused a slight desaturation of the rock which has now recovered. This interpretation is supported by the observation that the next electrode chain in the rock shows the same behaviour with a temporal delay (Figure 7-5). Near the deposition hole 6, no such effect was detected (Figure 7-6).

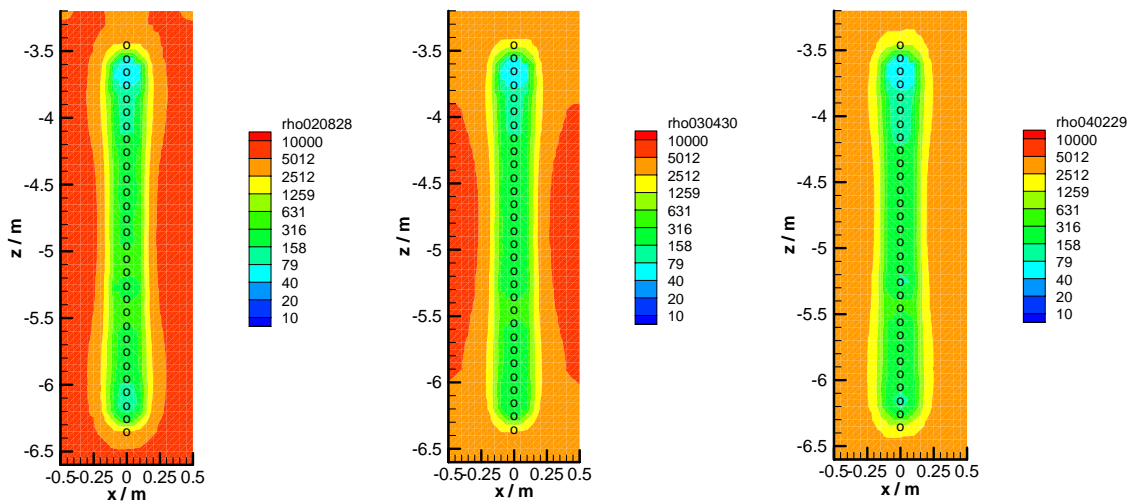


**Figure 7-4** Resistivity distribution in the rock around borehole KA 3550 G04 (near deposition hole 5), August 2002 (left), April 2003 (center), and February 2004 (right)

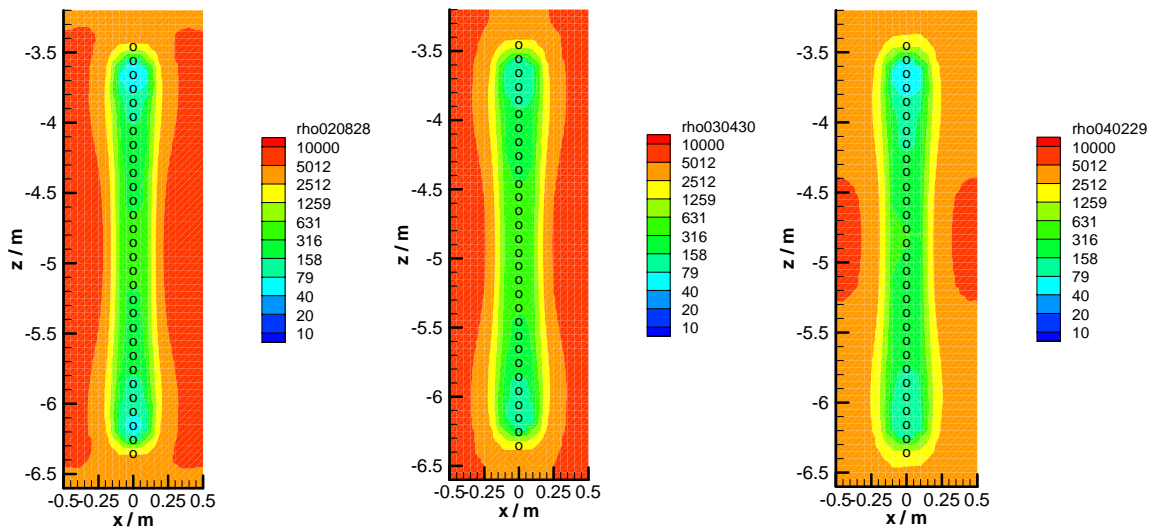


**Figure 7-5** Resistivity distribution in the rock around borehole KA 3549 G01 (between deposition holes 5 and 6), August 2002 (left), April 2003 (center), and February 2004 (right)

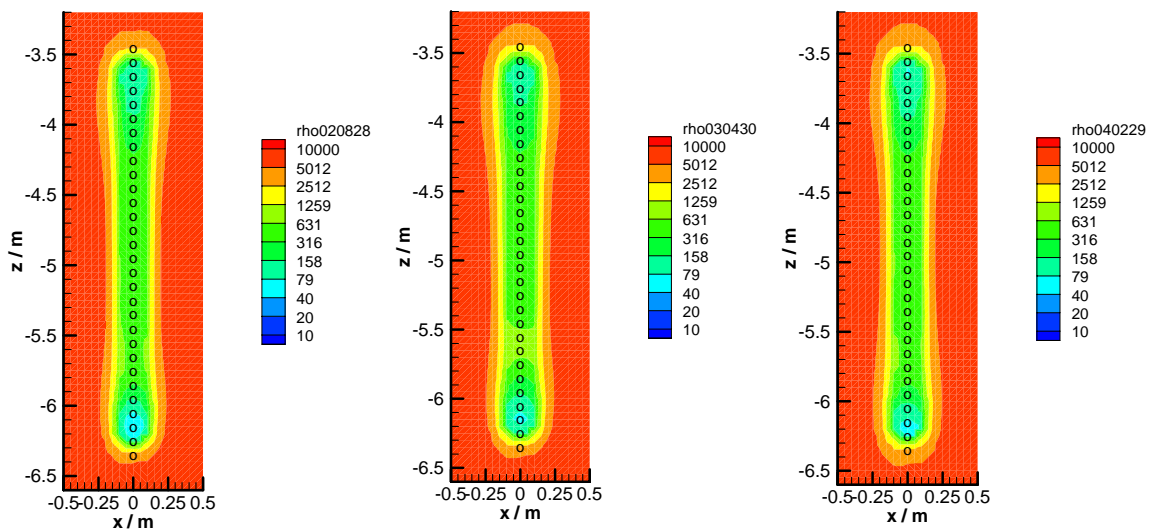


**Figure 7-6** Resistivity distribution in the rock around borehole KA 3546 G04 (near deposition hole 6), August 2002 (left), April 2003 (center), and February 2004 (right)

None of the measurements in the rock show any significant desaturation with time as a consequence of water uptake by the buffer. This supports the interpretation of the buffer measurements which hint to a water inflow to the buffer from the backfilled tunnel rather than from the borehole wall.

## 8 Summary and Conclusions

Within the framework of the Swedish nuclear programme, SKB has constructed a full-scale Prototype Repository at the Äspö Hard Rock Laboratory at a depth of 450 m below ground. The Prototype includes six deposition holes in which full-size canisters with electrical heaters have been placed and surrounded by a bentonite buffer. The deposition tunnel has been backfilled with a mixture of bentonite and crushed granitic rock.

Water uptake of the bentonite buffer in the deposition holes and of the bentonite/crushed rock backfill in the disposal gallery is one of the central issues to be investigated in the frame of the Prototype Repository Project performed at the Äspö URL. GRS uses the geoelectric method to determine the resistivity distributions in cross sections of the different materials.

In order to interpret the measured resistivities in terms of water content the resistivities of compacted MX-80 samples and of drift backfill were determined by laboratory investigations using the four-point method.

For the in-situ measurements in the Prototype Repository the automatic measuring system RESECS has been purchased. Tomographic dipole-dipole measurements have been performed in four electrode arrays distributed in the drift backfill, in the buffer at top of borehole 5, and in the rock between boreholes 5 and 6. The electrode chains consist of water-tight ELOCAB cables and GISMA plugs as well as of electrodes manufactured in GRS's workshop in Braunschweig.

The resistivities of the original buffer material were not significantly different to the resistivities of the backfill. Both the compacted MX-80 bentonite and the backfill show a very similar steep drop of the resistivity at the lower water contents. This can be explained by a clay-typical interface conductivity which is due to additional cations held loosely in the diffuse part of the electrical double layer surrounding the clay particles. Already a small amount of solution leads to formation of a double layer and causes the interface conductivity. The relatively small resistivity changes observed at higher saturation indicate that the interface conductivity is the predominant part of the conductivity in MX-80 bentonite. Because of the similar behaviour, it is furthermore concluded that the bentonite governs the resistivity behaviour of the backfill.

According to the laboratory results, the buffer and backfill will have already a rather small resistivity of about 7  $\Omega\text{m}$  and 13  $\Omega\text{m}$ , respectively when installed (at a water content of 12 to 13 wt.%). In conjunction with the comparably high resistivity of the rock (approx. 1000  $\Omega\text{m}$  at full saturation) it was feared that this might have the effect that resistivity reductions by increasing water uptake in the buffer could not be properly detected if the electrodes were located in the rock or rather close to the rock. In order to clear this issue, model calculations were performed in order to determine optimum electrode arrangements enabling high resistivity resolution. As a result of the analyses the electrode arrangement in the drift backfill was changed with respect to the original plans. The measurements in the buffer at top of borehole 5 have been performed by placing three electrode chains in the buffer and one chain in the rock. This arrangement was also a result of detailed model calculations.

Besides its dependence on the water content, the electrical resistivity is also a function of salinity and composition of the pore solution. Since both may change as the solution penetrates the buffer and the backfill, investigations were performed in order to quantify this effect.

For the investigation of solution composition changes during the penetration, Äspö-solution was applied to a 0.5 cm thin disk layer of compacted bentonite. In general it was concluded that at the beginning of the experiment the sample takes up Mg and Ca from solution while Na and K are being released. Dissolution of some minor components of MX-80 was also observed in the experiments. As the normality of percolate remains to be higher than that of Äspö-solution, this process seemingly remains to continue during the whole experiment. It cannot be explained with cation exchange.

However, the results show that under the given conditions of solution composition, flow velocity, compaction density, layer thickness, temperature and bentonite composition no salt retention is observed. The observed slight increase in salinity compared to the initial value for Äspö-solution does not indicate a significant change of electrical conductivity.

The results of the geoelectric measurements in the Prototype Repository obtained up to now show that the method is capable of monitoring water content changes in the backfill, the buffer, and the rock. The results are plausible and coherent.

The initial resistivity value of the backfill in October 2001 was about 10 to 14  $\Omega\text{m}$  corresponding to a water content of 13 to 14 %. In the following month the resistivity reduced to about 7 to 10  $\Omega\text{m}$  which corresponds to a water content of about 14 to 16 %. Until February 2004, a very homogeneous resistivity distribution is reached; with a value of 3 to 5  $\Omega\text{m}$  corresponding to a water content around 20 %.

The first measurement performed on June 18, 2003 in section 2 showed a much lower resistivity than the early measurements in section 1. Obviously, the backfill had a considerably higher water content already during installation. This observation was also made during instrumentation. Resistivity decreased farther away from the drift walls. Close to the walls it ranges now below 3  $\Omega\text{m}$ ; the backfill is therefore not far from full saturation. In the centre resistivity has decreased to values between 5 and 8  $\Omega\text{m}$  corresponding to a water content of about 15 to 18 %.

The results of the first measurement in the buffer of borehole 5 taken in May 2003 show the high resistivity (above 1000  $\Omega\text{m}$ ) of the rock on the right side and the low resistivity of the buffer (below 80  $\Omega\text{m}$ ) on the left. By taking up water, a progressing decrease of resistivity in the buffer was observed during the following months. In February 2004, the resistivity near the electrode chains was no longer higher than in the surrounding buffer. Near the electrode chain in the centre of the buffer, the resistivity ranged between 4 and 24  $\Omega\text{m}$ . The observation that the lowest resistivities are found near the top center of the buffer gives rise to the presumption that the water enters the buffer from the top, i. e., from the backfilled tunnel. In particular, there is no hint that significant amounts of water are drawn from the rock near the borehole wall into the buffer. This is confirmed by the measurements in the rock boreholes.

The resistivity distributions along the three electrode chains installed in the rock are quite similar to each other and show no significant variation in time until April 2003. Typical resistivity values of 2000 to 7000  $\Omega\text{m}$  were measured which are characteristic for granite. From April 2003 on, a slight decrease in resistivity in the rock near deposition hole 5 was observed. This coincides with installation of the buffer which also stopped the pumping of water from the open deposition hole. Apparently, this had caused a slight desaturation of the rock which has now recovered. This interpretation is supported by the observation that the next electrode chain in the rock shows the same behaviour with a temporal delay. Near the deposition hole 6, no such effect was detected.

The results of the geoelectric in-situ measurements show that it is possible to successfully use the method for detecting changes in water content of clay barriers. Although the resistivity changed only over a bandwidth of about 2 to 15  $\Omega\text{m}$  with the relevant water content variations, detection and reproduction of these variations was successful. It has, however, to be noted that detailed scoping calculations are indispensable to obtain an optimal electrode arrangement. Additionally, a good coupling of all electrodes to the investigated material is needed to get meaningful results.

## **9 Acknowledgements**

The work described in this report was funded by the Projektträger für Wasser-technologie und Entsorgung (PtWT+E) under contract No. 02 E 9279 and co-funded by the European Commission under contract No. FiKW-CT-2000-00055. The authors would like to thank for this support. Special thanks also to all project partners for their continuous support and the fruitful discussions in the many project meetings.

## 10 References

- Benzel, W. M.; Graf, D. L. (1984): Studies of smectite membrane behaviour: Importance of layer thickness and fabric in experiments at 20°C, *Geochim. Cosmochim. Acta* (48), 1769-1778.
- Dahlström, L.-O. (1998): Testplan for the Prototype Repository, Progress report HRL-98-24, Äspö Hard Rock Laboratory, SKB, Stockholm.
- Demir, I. (a) (1988): Studies of smectite membrane behaviour: electrokinetic, osmotic and isotopic fractionation at elevated pressures, *Geochim. Cosmochim. Acta* (52), 727-737.
- Demir, I. (b) (1988): The interrelation of hydraulic and electrical conductivities, streaming potential, and salt filtration during the flow of chloride brines through a smectite layer at elevated pressures, *Journal of Hydrology* (98), 31-52.
- DIN 18121-1: Baugrund, Untersuchung von Bodenproben - Wassergehalt- Teil 1: Bestimmung durch Ofentrocknung, Normenausschuss Bauwesen (NABau) im DIN Deutsches Institut, Normen e.V., April 1989
- Dresner, L.; Kraus, K. A. (1963): Ion exclusion and salt filtering with porous ion-exchange materials, *J. Phys. Chem.* (67), 990-996.
- Fechner, T. (2001) *SensInv2D-Manual*, Geotomographie, Neuwied.
- Goudarzi, R., Börgesson, L. (2003): Äspö Hard Rock Laboratory – Prototype Repository – Sensors data report (Period: 010917-030301), IPR-03-23, Svensk Kärnbränslehantering AB (SKB), Stockholm.
- Hanshaw, B. B.; Coplen, T. B. (1973): Ultrafiltration by a compacted clay membrane. II - Sodium ion exclusion at various ionic strengths, *Geochim. Cosmochim. Acta* (37), 2311-2327.

- Ishiguro, M.; Matsuura, T.; Detellier, C. (1996): A study on the solute separation and the pore size distribution of a montmorillonite membrane, *Sep. Sci. Technol.* (31/4), 545-556.
- Johnson, K. S. (1979): Ion association and activity coefficients in electrolyte solutions, Ph. D. Thesis, Oregon State University.
- Johnson, K. S. (1981): The calculation of ion pair diffusion coefficients: a comment, *Mar. Chem.* (10), 195-208.
- Kemna, A. (1995) Tomographische Inversion des spezifischen Widerstandes in der Geoelektrik, Master Thesis, Universität Köln.
- Kemper, W. D.; Evans, N. A. (1963): Movement of water as affected by free energy and pressure gradients III. Restriction of solutes by membranes, *Soil Sci. Soc. Am. Proc.* (27), 485-490.
- Kemper, W. D.; Maasland, D. E. L. (1964): Reduction in salt content of solution on passing through thin films adjacent to charged surfaces, *Soil Sci. Soc. Am. Proc.* (28), 318-323.
- Kharaka, Y. K.; Berry, F. A. F. (1973): Simultaneous flow of water and solutes through geological membranes - I. Experimental investigation, *Geochim. Cosmochim. Acta* (37), 2577-2603.
- Kharaka, Y. K.; Smalley, W. C. (1976): Flow of water and solutes through compacted clays, *Am. Assoc. Petr. Geol. Bull.* (60/6), 973-980.
- Kull, H.; Flach, D.; Graefe, V. (2001): Untersuchung physikalischer Prozesse und Parameter zum Fluid- und Gastransport im Nahbereich von Endlagern in einer homogenen granitischen Gesteinsmatrix, Abschlussbericht zum gleichnamigen Forschungsprojekt des BMFT, FKZ 02 E 8151 A8, Gesellschaft für Anlagen- und Reaktorsicherheit mbH, GRS-172.
- Marshall, C. E. (1948): The electrochemical properties of mineral membranes. The theory of selective membrane behaviour, *J. Phys. Chem.* (52), 1284-1295.

Serra, O.: Fundamentals of well-log interpretation. 1. The acquisition of well logging data. (Development in petroleum science 15A), Elsevier; Amsterdam - Oxford - New York - Tokyo 1984).

Schick, R. and Schneider, G. (1973): Physik des Erdkörpers - Eine Einführung für Naturwissenschaftler und Ingenieure, Ferdinand Enke Verlag Stuttgart.

Schopper, J. R.: Electrical conductivity of rock containing electrolytes. In: Landolt-Börnstein, Numerical Data and Functional Relationships in Science and Technology. New Series edited by K.-H. Hellwege, Groupe V: Geophysics and Space Research, Volume 1, Physical properties of Rocks, subvolume b, edited by G. Angenheiser., Springer-Verlag Berlin, Heidelberg, New York 1982

Sposito, G. (1989): The Chemistry of Soils, Oxford University Press.

## List of Figures

Figure 3-1	Principle configuration of a dipole-dipole measurement.....	7
Figure 3-2	Front view of RESECS measuring system.....	11
Figure 3-3	Rear view of RESECS measuring system.....	12
Figure 3-4	Screen display of RESECS measuring software.....	16
Figure 4-1	Overview of electrode arrangements in the Prototype Repository .....	17
Figure 4-2	Double cross electrode arrangement in the backfill.....	19
Figure 4-3	Electrode chains at top of borehole 5 .....	20
Figure 4-4	Design of electrode chains in the rock, showing the upper chain used for the buffer measurements and the lower chains for monitoring the rock .....	21
Figure 4-5	Design of an ELOCAB-cable (diameter of multiwire cable: 27.5 mm, diameter of single wire: 2.7 mm) .....	22
Figure 4-6	GISMA-plug .....	22
Figure 4-7	Principle design of an electrode chain in the drift.....	23
Figure 4-8	Design of a drift electrode.....	24
Figure 4-9	Design of electrode chain in the buffer .....	24
Figure 5-1	Schematic view of the resistivity measurement cell for compacted MX-80 samples .....	28
Figure 5-2	Schematic experiment layout for the determination of sample resistivity (4-point method) .....	30
Figure 5-3	Resistivity of compacted MX-80 samples and original ÄSPÖ buffer material as a function of the water content.....	31
Figure 5-4	Emplacement of moisturized backfill into measurement cell for determination of material resistivity .....	35
Figure 5-5	Measurement set-up for determination of backfill resistivity.....	35
Figure 5-6	Resistivity of compacted backfill samples versus water content .....	36
Figure 5-7	Exsiccator with granite rock samples .....	37

Figure 5-8	Schematic of the 2-point arrangement for the determination of the resistivity .....	38
Figure 5-9	Measurement set-up for determination of clay rock resistivity.....	38
Figure 5-10	Sample coated with conductivity silver lacquer .....	39
Figure 5-11	Resistivity of granite at different saturations and temperatures.....	40
Figure 5-12	Experimental set-up of percolation experiment .....	46
Figure 5-13	Composition of Äspö solution. All concentrations in mg/l. ....	47
Figure 5-14	Change of normality of percolate. Note that normality is constantly a bit higher than that of inflowing solution .....	49
Figure 5-15	Na-concentration in Äspö-solution after penetrating compacted MX-80 .....	49
Figure 5-16	K-concentration in Äspö-solution after penetrating compacted MX-80 .....	50
Figure 5-17	Mg-concentration in Äspö-solution after penetrating compacted MX-80 .....	50
Figure 5-18	Ca-concentration in Äspö-solution after penetrating compacted MX-80 .....	51
Figure 5-19	Cl-concentration in Äspö-solution after penetrating compacted MX-80 .....	51
Figure 5-20	SO <sub>4</sub> -concentration in Äspö-solution after penetrating compacted MX-80 .....	52
Figure 5-21	Mineral saturation states in percolates .....	55
Figure 6-1	Geoelectric modelling of the prototype repository backfill: Rectangular model without surrounding rock (left: input model, right: inversion result) .....	58
Figure 6-2	Geoelectric modelling of the prototype repository backfill: Rectangular model with surrounding rock (left: input model, right: inversion result) .....	59
Figure 6-3	Geoelectric modelling of the prototype repository backfill: Elliptic drift model with surrounding rock (left: input model, right: inversion result); "double cross" electrode arrangement (x = electrode locations) .....	59
Figure 6-4	Geoelectric modelling of the prototype repository buffer with the original electrode arrangement (left: input model, right: inversion result) .....	60

Figure 6-5	Geoelectric modelling of the prototype repository buffer with additional central chain (left: input model, right: inversion result).....	60
Figure 6-6	Geoelectric modelling of the prototype repository buffer with additional horizontal chain (left: input model, right: inversion result).....	61
Figure 6-7	Geoelectric modelling of the prototype repository buffer with the new electrode arrangement: dry buffer (left: input model, right: inversion result) .....	61
Figure 6-8	Geoelectric modelling of the prototype repository buffer with the new electrode arrangement: partially wetted buffer (left: input model, right: inversion result).....	62
Figure 6-9	Geoelectric modelling of the prototype repository buffer with the new electrode arrangement: enlarged wet buffer zone (left: input model, right: inversion result).....	62
Figure 7-1	Resistivity distribution in Backfill Section I, October 2001 (upper left), September 2002 (upper right), August 2003 (lower left), and February 2004 (lower right) .....	64
Figure 7-2	Resistivity distribution in Backfill Section II, June 2003 (left) and February 2004 (right).....	65
Figure 7-3	Resistivity distribution in the buffer at the top of deposition hole 5, May 2003 (left) and February 2004 (right) .....	66
Figure 7-4	Resistivity distribution in the rock around borehole KA 3550 G04 (near deposition hole 5), August 2002 (left), April 2003 (center), and February 2004 (right).....	67
Figure 7-5	Resistivity distribution in the rock around borehole KA 3549 G01 (between deposition holes 5 and 6), August 2002 (left), April 2003 (center), and February 2004 (right) .....	68
Figure 7-6	Resistivity distribution in the rock around borehole KA 3546 G04 (near deposition hole 6), August 2002 (left), April 2003 (center), and February 2004 (right).....	68

## List of Tables

Table 5-1	Composition of the used Äspö-solution [mmol/l] .....	27
Table 5-2	Water content and size of the prepared MX-80 samples and of the original buffer samples .....	29
Table 5-3	Summary of the water content and the resistivities of the compacted MX-80 samples and the original Äspö buffer material.....	32
Table 5-4	Water content and achieved dry density of backfill samples .....	33
Table 5-5	Investigated mixtures of cementation materials .....	41
Table 5-6	Summary of the results of granite-cement and sand-cement mixtures produced with an ÄSPÖ-specific solution stored at wet conditions.....	44
Table 5-7	Planning data for percolation experiment .....	48

**Gesellschaft für Anlagen-  
und Reaktorsicherheit  
(GRS) mbH**

Schwertnergasse 1  
**50667 Köln**  
Telefon +49 221 2068-0  
Telefax +49 221 2068-888

Forschungsinstitute  
**85748 Garching b. München**  
Telefon +49 89 32004-0  
Telefax +49 89 32004-300

Kurfürstendamm 200  
**10719 Berlin**  
Telefon +49 30 88589-0  
Telefax +49 30 88589-111

Theodor-Heuss-Straße 4  
**38122 Braunschweig**  
Telefon +49 531 8012-0  
Telefax +49 531 8012-200

**[www.grs.de](http://www.grs.de)**